Area Law Violations in Entanglement Measures for Spatially Inhomogeneous Quantum Spin Chains

AC38091

September 2022

Abstract

In this report, we investigate entanglement scaling in one dimensional, inhomogeneous quantum spin chains. In particular, we reproduce findings on entanglement entropy and logarithmic negativity in spatially inhomogeneous systems, and extend the analytical results to systems couplings that decay slowly from the centre. We verify these results with the strong disorder renormalisation group (SDRG) method and with the exact solution where possible. We show that with slowly decaying couplings, the area law violation is maintained but we cannot yet describe it well quantitatively.

Contents

1 Introduction

Entanglement is often regarded as the stylistic feature of quantum systems [1]. A significant amount of work has gone into quantifying the scaling of the entanglement entropy $S(\rho_A)$:

$$S(\rho_A) = -\operatorname{Tr}(\rho_A \log \rho_A) \tag{1.1}$$

and of the logarithmic negativity $\mathcal{E}(\rho_A)$:

$$\mathcal{E}(\rho_A) = \ln ||\rho_A^{T_2}|| \tag{1.2}$$

of a subsystem defined by a reduced density matrix ρ_A. This report will extend the work of two papers ([1] and [2]) which quantified the scaling of both of these measures in quantum spin chains. In particular, the authors studied the entanglement scaling of spin chains with varying degrees of heterogeneity: in systems with inhomogeneity introduced via disorder and in 'exponential' systems where, along with a disordered factor, the couplings contain a second factor which decays from the centre of the chain. Their research was motivated by the pre-existing knowledge of area law violations for entropy in quantum systems. Eisert et al. [3] list four important motivations for studying the scaling of entanglement:

1. Black hole physics: Beckstein-Hawking radiation is proportional to the boundary of the black hole [4].

2. The theory of long range quantum correlations - understanding area laws and their violations will give a greater understanding of how quantum correlations are distributed within a many-body system.

3. Complexity of numerical simulations: great success has been made in classical physics through mean field theory to more efficiently solve complex systems ([5]). If we understand how and when mean field theories work for quantum systems, this will help us to effectively solve complex quantum systems.

4. Topological entanglement entropy, a novel order parameter, cannot be described by local conditions.

For example, it is known that for local, gapped, spatially invariant one dimensional quantum systems in their groundstate, entanglement entropy must scale with an area law [6]. However, attempts to generalise this to weaker conditions have shown that violations to the area law can occur [7]. Thus a research programme has begun to study which violations of the assumptions in [6] are necessary or sufficient to lead to such violations. Subsequent papers ([8], [1], [2]) have developed a significant number of results.

The presence of disorder introduces a new richness of modelling possibilities but also creates serious technical problems. In particular, spatial homogeneity is violated and this loss of symmetry makes solving the models more difficult. This has prompted a wave a numerical techniques based on renormalisation group theory ([9], [7]). Further complicating the picture is the presence of interactions. The combination of disorder and interactions makes disordered quantum chains truly complex systems: there are no known analytical solutions to the interacting disordered spin chain [1]. We will implement some analytical results, but to facilitate analysis we use the Strong Disorder Renormalisation Group (SDRG) technique for the majority of our calculations. The SDRG technique is useful for understanding the groundstate of disordered systems and is known to be asymptotically exact [7]. We implement algorithms for the SDRG procedure and associated analyses, as well as for the exact solutions where possible, at arbitrary precision.

In this report, we will frequently refer to a 'subsystem' centred in a one dimensional chain frequently, so we will disambiguate that term here. We present in figures 1.1 and 1.2, the two key subsystem scenarios. In figure 1.1, we show a single subsystem A in the centre of the chain. The details of the setup will depend on the boundary conditions and the parity of the system length L - in

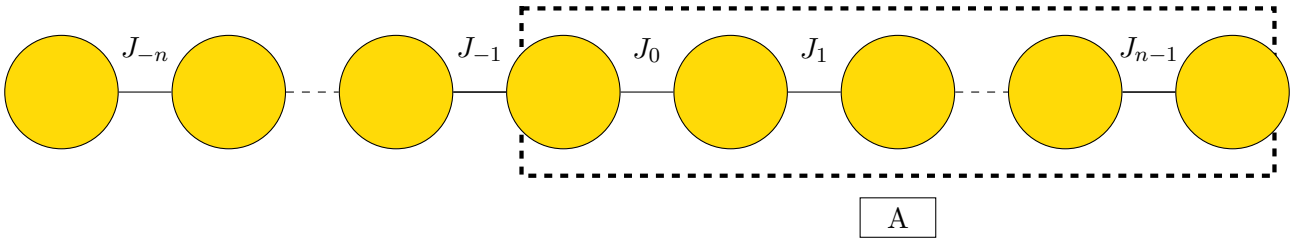

Figure 1.1: A chain of spins with the central spin labelled J_0. The subsystem A is highlighted with the dashed line. Unless otherwise stated, subsystems will always start from the centre of the chain.

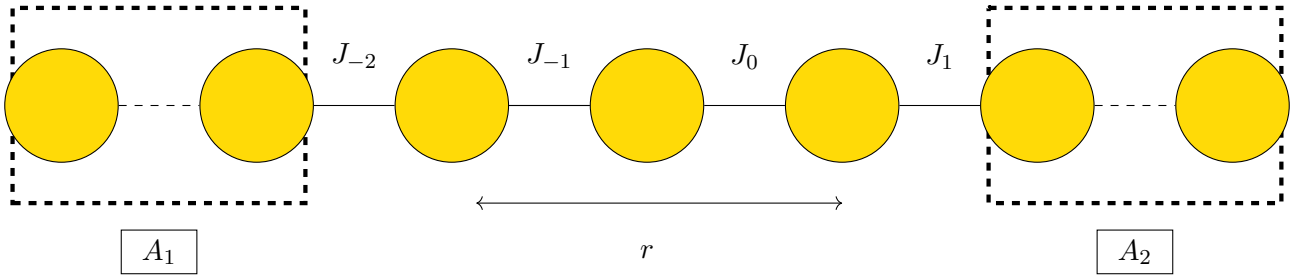

Figure 1.2: A chain of spins with a pair of disjoint subsystems, separated by a distance r. The subsystems A_1 and A_2 are highlighted with the dashed line. Unless otherwise stated, subsystems will always start from the centre of the chain.

particular, whether J_0 is in the centre of the chain or to the right hand side of the central coupling. In figure 1.2, we show two disjoint subsystems separated by a region r, which will normally be restricted to even length. Again, the exact implementation will depend on the boundary conditions and the parity of the system's length.

Throughout, we will use J_i to refer to the i^{th} site as well as the bond immediately to the right of said bond. In ambiguous cases we will clarify things accordingly. In the case of periodic boundary conditions, the bond extending from site L will connect around into site 1. In open boundary conditions, spin L will have a bond $J_L = 0$ which effectively eliminates that interaction from the system.

The structure of the rest of this report is as follows. In section 2, we review the current literature around entanglement measures and area law violations in quantum systems. In section 3, we will briefly summarise the history of the renormalisation group theory and SDRG, and lay out the spin chain models to be investigated and the SDRG procedure. In section 4, we will outline the implementation of the SDRG procedure and demonstrate some initial verifications and time benchmarks. In section 5 we will verify some existing results for area law violations, and in sections 6 and 7, we will demonstrate the new results on entanglement negativity for old systems and for the new slowly decaying systems. Lastly, in section 8 we will evaluate the new results and discuss areas for further research. In the appendix, we review basic quantum physics and and the Jordan-Wigner transformation.

2 Measures of Entanglement

2.1 Entanglement as a Information Phenomenon

Entanglement is a type of correlation unique to quantum mechanics, but calculating the amount of correlation is difficult. One approach is the 'operational approach' [10], which says that states are entangled if and only if (iff) they are *seperable*. Separability implies that, given a set $\{p_i\}$, and a similar set of density matrices for two subsystems A and B, the final density matrix ρ can be written as:

$$\rho = \sum_i p_i \rho_A^i \otimes \rho_B^i \tag{2.1}$$

Thus a first (and incorrect) attempt would be to define entanglement as 'the property of any statement that cannot be reached by local operations and classical communication' (LOCC). LOCC includes, for example, experiments on quantum systems to take observations, and traditional methods of communication. However, as Peres shows [11], LOCC is only a subset of operations that lead to separable states. Rather, density matrices must be at least *positive partial transpose preserving* (PPT preserving): this is known as the Peres criterion. The partial transpose is defined as follows - given a density matrix ρ defined as:

$$\rho = \sum_{ijkl} p_{kl}^{ij} |i\rangle \langle j| \otimes |k\rangle \langle l| \tag{2.2}$$

then the partial transpose with respect to B is:

$$\rho = \sum_{ijkl} p_{kl}^{ij} |i\rangle \langle j| \otimes (|k\rangle \langle l|)^T \tag{2.3}$$

The preceding matrix is positive iff it does not have any negative eigenvalues.

However, even the Peres criterion does not guarantee that the the partial transpose of the density matrix is positive [10], so LOCC presents a useful heuristic for defining a set of axioms that any measure of entanglement must satisfy [12].

An excellent review of measures of entanglement is [13], section two, and [14]. We will focus here on operational view, which measures entanglement in a way that is physically intuitive, and the mathematical approach that seeks rigorous and numerically stable measures ([10], [15]). For example, the entanglement of distillation gives the number of maximally entangled pairs that can be purified from a quantum state [16]. Yet purification processes are varied and there is not yet a way of calculating this quickly. On the other hand, negativity (see section 2.2 for a definition) is well defined but does not have any obvious physical interpretation.

In Vedral et al. 1997 they present a set of axioms for entanglement to satisfy [12] in order to provide a rigorous grounding. This is in response to the fact that states had been found that did not violate the Clauser-Horne-Shimony-Holt (CHSH) inequality (i.e. they did not appear to be entangled) but that were effectively entangled under local operations and classical communication (LOCC, again see section 2.1) [17]. In light of the debate around what the most suitable set of axioms for defining entanglement should be, we follow [10] and use the following three necessary conditions for a measure of entanglement E:

1. *Monotonicity*: $E(\rho) \geq \sum_i E(\Theta(\rho))$ for some LOCC operation Θ
2. *Convexity*: $\sum_i p_i E(\rho_i) \geq E\left(\sum_i p_i \rho_i\right)$
3. *Additivity under the tensor product*: $E\left(\otimes_i \rho_i\right) = \sum_i E\left(\rho_i\right)$

Mathematically, perhaps the most important criteria for any measure of entanglement is that it is monotone ([15], [10]), which implies that any classical interference with the state (represented by the operation Θ) can only lower its entropy. This is one requirement for keeping measures of entanglement focused strictly on the quantum correlations. The convexity requirement is more contentious. The right hand side of the convexity condition describes a *mixed state*, i.e. a classical combination of

quantum states. The convexity condition implies that a classical mixing of states cannot produce entanglement, which is prima facie a desirable property of an entanglement measure. However, Plenio shows that for entanglement negativity the monotonicity requirement is sufficient to guarantee its suitability as a measure of entanglement because 'convexity is merely a mathematical requirement for entanglement monotones and generally does not correspond to a physical process describing the loss of information' [15]: essentially Plenio does not agree that convexity needs to be in the list of entanglement axioms as monotonicity is sufficient. The additivity requirement is exceptionally useful as it allows the calculation of product states, including the random singlet phase that will be discussed in 3.3.

To summarise, defining measures of entanglement that satisfy all of the axioms one could reasonably wish for is difficult - in this report we focus on entanglement entropy and entanglement negativity, which we define in the following section.

2.2 Entanglement Entropy and Negativity

We will now define the key measures of entanglement used in this report. We define the generalised Rényi entropies:

$$S_n(\rho_A) = \frac{1}{1-n} \log \operatorname{Tr} \rho_A^n \tag{2.4}$$

where ρ_A is the reduced density matrix over the subsystem A, found by taking the partial trace over the B subsystem with bases $|j_B\rangle$:

$$\rho_A = \operatorname{Tr}_B[\rho] = \sum_j \langle j|_B \, \rho \, |j\rangle_B \tag{2.5}$$

Rényi entropies were introduced in [18] as a generalisation of Shannon entropies to quantum systems. Whilst Rényi entropies capture meaningful quantum correlations, they do not satisfy the useful subadditivity condition:

$$S(\rho_{A\cup B}) \leq S(\rho_A) + S(\rho_B) \tag{2.6}$$

for bipartite systems $A \cup B$. Fortunately, taking the limit $n \to 1$ we recover the von Neumann entanglement entropy 1.1, which is subadditive [19]. Note that all Rényi entropies are symmetric with respect to the subsystem, i.e. $S_n(\rho_A) = S_n(\rho_B)$ [10], which also suggests that an area law would be reasonable to expect: if $|A| > |B|$, it would be odd for $S(\rho_A) = S(\rho_B)$ if entropy scaled with volume.

Unfortunately, the entanglement entropy is only measurable if the system is in a pure state and if it is bipartite [10]. The only other measurable form of entanglement is the *negativity*. Before defining negativity, we define the *partial trace*:

$$\langle \varphi_A \varphi_B | \rho_A^{T_2} | \varphi'_A \varphi'_B \rangle \equiv \langle \varphi_A \varphi'_B \, | \rho_A | \, \varphi'_A \varphi_B \rangle \tag{2.7}$$

where $\{\varphi_X\}$ is a basis for subsystem X [1]. We also define the trace distance $||A||$ of a generic operator A:

$$||A|| = \operatorname{Tr} \sqrt{AA^\dagger} \tag{2.8}$$

Assuming A is Hermitian, the trace distance of A is the sum of the absolute value of the eigenvalues of A [10]. Given the discussion about the Peres criterion, it is clear that this quantity measures the negativity of the partially transposed density matrix. We can now define the negativity:

$$\mathcal{N}(\rho_A) = \frac{||\rho_A^{T_2}|| - 1}{2} \tag{2.9}$$

Whilst this is monotone [20], it is not additive under the tensor product. However, we can take the logarithm and neglect the constant factors to get the logarithmic negativity (equation (1.2), which is additive under the tensor product.

2.3 Area Law Violations in Quantum Systems

We will briefly survey the wide literature of area law violations in quantum systems. For a thorough review, we recommend [3]. Early work on the scaling of entropy in quantum systems focused on the study of blacks holes: in particular, Bombelli et al. [21] and Srednicki [22]. As discussed in section 1, the event horizon of a black hole and the theory of Hawking radiation are of great general interest. Srednicki argued that for a field of quantum harmonic oscillators divided into a spherical 'in' region and exterior, the entropy of the 'in' region must scale with the area as opposed to the volume, as the surface area is the only region common to both subregions. In 2004 Hastings published a proof of the area law for local, gapped, translationally invariant systems in one dimension in the their groundstate [6], e.g. Hamiltonians of the form:

$$H = \sum_{i=1}^{N} H_{i,i+1} \tag{2.10}$$

where $H_{i,i+1}$ is a function only of the sites i and $i+1$. Note that this applies strictly to systems in their groundstate - for example, Page [23] shows that if a system is in a random pure state, the average entropy of the subsystem scales as a volume law.

This 'area law' sets the baseline for the physics of such systems: any evidence of violations to this area law must also explain how to account for this violation. Many theoretical systems do in fact display area law violations of their quantum entropy [24], and thus a literature has sprung up to identify and explain these phenomena with a variety of tools. For example, in a very detailed survey Calabrese and Cardy [25] give a thorough treatment through $(1+1)d$ conformal field theory (CFT) of the entanglement entropy, and show that the entropy S_A of a subsystem A of length l at zero temperature in an infinitely long, 1D system without boundaries is:

$$S_A \sim (c/3) \log (l/a) \tag{2.11}$$

where c is the central charge and a is the lattice spacing. This is known as a logarithmic correction to the area law. Similarly, Calabrese et al. compute the scaling of the logarithmic negativity in the CFT framework [26].

In the following section we will outline the principle model that we study as well as the SDRG procedure. This will also allows us to explain how entropy measures are calculated in the simulations we conduct.

3 The Random Inhomogeneous Chain and the SDRG method

3.1 Random Inhomogeneous 1D Chain

The random inhomogeneous spin-$\frac{1}{2}$ XXZ chain with L spins and open boundary conditions (OBC) has the Hamiltonian:

$$H = \sum_{i=1}^{L-1} J_i \left(S_i^x S_{i+1}^x + S_i^y S_{i+1}^y + \Delta S_i^z S_{i+1}^z \right) \tag{3.1}$$

where $S_i^x = \frac{\hbar}{2}\sigma_x$ and σ_i^x is a Pauli matrix acting on site i, J_i is a random coupling connecting site i to $i+1$, and Δ is an anisotropy parameter. For periodic boundary conditions (PBC) an additional term for $i = L$ is needed. With $\Delta = 1$ we have the XXX chain and with $\Delta = 0$ we have the XX chain. With the XX chain the model is analytically solvable [1].

More details of how the couplings $\{J_i\}$ are calculated will be given in more detail in the relevant sections. Here we will give the most general form of the couplings:

$$J_i = K_i \times F(i) \tag{3.2}$$

where F is function that depends deterministically on i, and K_i is a random variable with the following distribution:

$$P_\delta(J) \equiv \delta^{-1} J^{-1+1/\delta} \tag{3.3}$$

Clearly as $\delta \to 0$ the disordered contributions tend to 1 and taking $F(i) = 1$ we recover the clean spin chain. For $\delta \to 1$ we approach a uniform distribution on $[0, 1]$. As $\delta \to \infty$ we approach the infinite randomness fixed point (IRFP), which describes the asymptotic state of the distribution of $\{J_i\}$ under successive SDRG steps (see 3.4) [9].

3.2 SDRG Literature Review

Whilst in non-interacting cases, one dimensional spin chain models are often analytically solvable, this is not the case in general. The renormalisation group (RG) approach to approximating complex systems (quantum and classical) came out of work with (Michael) Fisher and Wilson in the 1960s [27]. RG involves successively integrating out the high energy degrees of freedom in a model to approach an approximation of the system's groundstate. Each RG step f maps the problem $H(J)$ to a new problem $f(H(J)) = H(J')$ with fewer degrees of freedom. Iterating this process will lead to a point where the transformation $f(H(J^\star)) = H(J^\star)$ is a fixed point.

In this paper we will focus on disordered models, for which we use the strong disorder renormalisation group (SDRG). For a very thorough review, see [28] and [29]. Studies of disordered systems start as early as 1968 [30], and the key contribution was from Dasgupta, Ma, and Hu ([31], [32]) who defined a rule for the elimination of bonds that was generalised by (Daniel) Fisher [9]. Since then the SDRG procedure has been used to investigate a great variety of challenging disordered problems ([33], [34], [35], [7], [8], [1], [2]).

The SDRG procedure is often used alongside matrix product states, and in particular to the density matrix renormalisation group (DMRG)[36]. For a thorough review, see [37] and [38]. A detailed discussion of the literature on DMRG is beyond the scope of this report, but it is worthwhile out that in [1], the DMRG technique struggled to converge for large system size L, with significant errors relative to the exact solution (where exact solutions were available). For this reason we have not used the DMRG method in this report.

3.3 SDRG Procedure

We will summarise the SDRG procedure for the inhomogeneous 1D spin chain following [1]. To begin with, we identify the strongest coupling J_M and consider the energy of this interaction H_0:

$$H_0 = J_M \vec{S}_l \cdot \vec{S}_r \tag{3.4}$$

The groundstate of this microsystem is:

$$|s\rangle \equiv 2^{-1/2} \left(|\uparrow_l \downarrow_r\rangle - |\downarrow_l \uparrow_r\rangle \right) \tag{3.5}$$

where $\{\uparrow_l, \downarrow_r\}$ are up and down basis vectors for the single spin Hilbert space. Treating this as a perturbation[1], we can calculate a new effective coupling between the spins $l-1$ and $r+1$:

$$J' = \frac{J_l J_r}{(1+\Delta) J_M} \tag{3.6}$$

We remove the spins connected by J_M and insert the coupling J' between J_l and J_r. The removed spins are recorded in a list that will be the random singlet phase result of the SDRG procedure. Repeating this process identifies a flow of couplings between steps:

$$(\cdots, J_l, J_M, J_r, \cdots)_L \to \left(\cdots, \frac{J_l J_r}{(1+\Delta) J_M}, \cdots \right)_{L-2} \tag{3.7}$$

Importantly, given that $J_M > J_{(l/r)}$, the new coupling J' is smaller than either, the energy scale of the model is lowered.

By the end of the procedure, we are left with a list of $L \div 2$ singlets. Calling this vector of singlets $\{|s\rangle_i\}$, the groundstate as approximated by the SDRG procedure is:

$$|GS\rangle = \bigotimes_{i=1}^{L \div 2} |s\rangle_i \tag{3.8}$$

3.4 SDRG Flow

The resulting distribution of couplings in terms of the SDRG step m can be given quantitatively, following [9]. We introduce the logarithmic variables:

$$\beta_i^{(m)} \equiv \ln \frac{J_M^{(m)}}{J_i^{(m)}}, \quad \Gamma^{(m)} \equiv \ln \frac{J_M^{(0)}}{J_M^{(m)}} \tag{3.9}$$

where $J_M^{(m)}$ is the strongest coupling at the SDRG step m. The flow equation to be solved is given by [9] as:

$$\frac{dP}{d\Gamma} = \frac{\partial P(\beta)}{\partial \beta} P(0) \times \int_0^\infty d\beta_1 \int_0^\infty d\beta_2 \delta \left(\beta - \beta_1 - \beta_2 \right) P\left(\beta_1\right) P\left(\beta_2\right) \tag{3.10}$$

which is solved with the ansatz:

$$P^*(\beta) = \frac{1}{\Gamma} \exp\left(-\frac{\beta}{\Gamma} \right) \tag{3.11}$$

Equation 3.10 is an attractor for any initial distribution of the couplings.

As an initial test of the SDRG procedure we implemented, we have tracked the flow of the logarithmic couplings in figure 3.1. This is a close reproduction of a similar figure in [1] and shows that the SDRG process is indeed working correctly.

[1] Details of the perturbation calculations can be found in [1] as well.

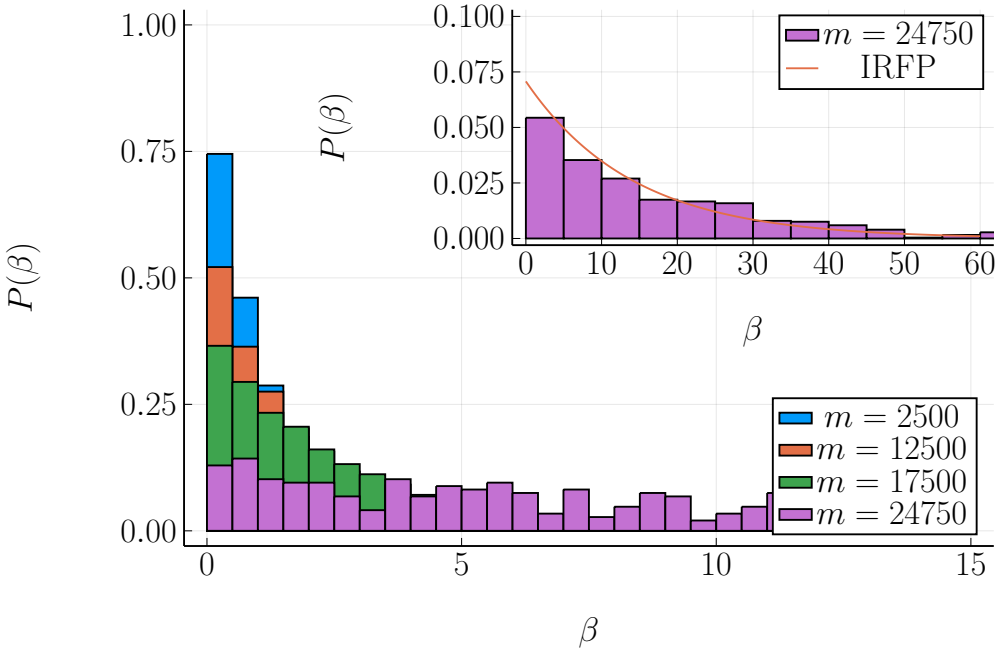

Figure 3.1: SDRG flow for $L = 50,000$ spins in the disordered XXX chain where $\delta = 1$. The main plot shows the β distribution of the remaining bonds at the m^{th} step of the SDRG process. Notice that over SDRG steps, the distribution approaches the IRFP. The inset plot shows subset of the β distribution late into the SDRG process with the IRFP line overlayed. The data is an excellent fit to the analytical prediction.

3.5 Calculating Entropy in the 1D Chain

In this section we will explain how the entanglement entropy and logarithmic negativity can be calculated. We observe that, given the RSP state in equation 3.8, we can calculate the entanglement measures of a subsystem A just by focusing on the singlet states in A.

For the entanglement entropy, we only need to know the number of singlets in A that connect to the remainder of the chain $B = A'$. Each singlet can be constructed as follows - in the basis $|\uparrow\rangle = \begin{bmatrix} 1 \\ 0 \end{bmatrix}$ and $|\downarrow\rangle = \begin{bmatrix} 0 \\ 1 \end{bmatrix}$ we can make the singlet state $|s\rangle$ (see equation 3.5) explicit:

$$\rho = |s\rangle \langle s| = \frac{1}{2} \begin{pmatrix} 0 & 0 & 0 & 0 \\ 0 & 1 & -1 & 0 \\ 0 & -1 & 1 & 0 \\ 0 & 0 & 0 & 0 \end{pmatrix} \tag{3.12}$$

Taking the partial trace over the second spin, we have:

$$\rho_A = \frac{1}{2} \begin{pmatrix} 1 & 0 \\ 0 & 1 \end{pmatrix} \tag{3.13}$$

To calculate the entanglement entropy, we use the spectral theorem on equation 1.1 to get:

$$S_A = -\sum_i \lambda_i \ln \lambda_i = \ln 2 \tag{3.14}$$

where $\{\lambda_i\}$ are the eigenvalues of ρ_A. Following [7], the entanglement entropy is just 'the number of singlets that connect sites inside to sites outside the segment', multiplied by the entropy of each such segment, $\ln 2$. We follow [1] and let the number of singlets connecting subsystem X to Y be $n_{X:Y}$, so that the entropy $S_A = \ln 2 \times n_{A:B}$.

For the entanglement entropy, we require a more involved approach. We note that the groundstate as described in equation 3.8 is a tensor product of singlet states, and that from section 2.2 the

logarithmic negativity is additive under the tensor product. Before we go further it is useful to call the generic singlet density matrix ρ_{2S} and to note that partial trace of this is:

$$\rho_{2S}^{T_2} = \frac{1}{2}\begin{pmatrix} 0 & 0 & 0 & -1 \\ 0 & 1 & 0 & 0 \\ 0 & 0 & 1 & 0 \\ -1 & 0 & 0 & 0 \end{pmatrix} \tag{3.15}$$

This is achieved in this simple case by transposing each 2×2 block of the matrix in equation 3.12. Furthermore, distinguishing between singlets which connect A to A, B to B, and A to B, we can follow [1] and describe the complete RSP as:

$$\rho_{RSP} = \bigotimes_{i=1}^{n_{A:A}} \rho_{2S} \bigotimes_{i=1}^{n_{B:B}} \rho_{2S} \bigotimes_{i=1}^{n_{A:B}} \rho_{2S} \tag{3.16}$$

We then trace over the B subsystem, leaving us with:

$$\rho_A = \bigotimes_{i=1}^{n_{A:A}} \rho_{2S} \bigotimes_{i=1}^{n_{A:B}} \rho_S \tag{3.17}$$

and after taking the partial transpose:

$$\rho_A^{T_2} = \bigotimes_{i=1}^{n_{A:A}} \rho_{2S}^{T_2} \bigotimes_{i=1}^{n_{A:B}} \rho_S^{T_2} \tag{3.18}$$

The logarithmic negativity is additive over this, and according to [1] it simplifies to:

$$\mathcal{E}_{A_1:A_2} = n_{A_1:A_2} \ln \mathrm{Tr} \left| \rho^{T_2} \left(A_1 \cup A_2 \right) \right| \tag{3.19}$$

where ρ is the density matrix of the generic singlet state. As discussed in section 2.2, the trace norm of a Hermitian matrix is just the some of the absolute value of its eigenvalues. The eigenvalues of $\rho_{2S}^{T_2}$ are $\{-1/2, 1/2, 1/2, 1/2\}$, thus the trace norm is 2 and the logarithmic negativity of the total subsystem A is:

$$\mathcal{E}_{A_1:A_2} = n_{A_1:A_2} \ln 2 \tag{3.20}$$

This simply says that the entanglement negativity of the subsystem is $\ln 2$ multiplied by the number of singlets shared between A_1 and A_2.

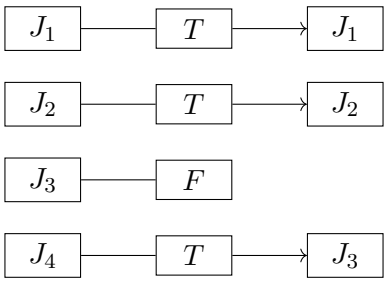

Figure 4.1: Diagram of the data masking procedure used to iteratively eliminate the bonds from the data vector. The approach is size stable so minimises the need for allocations during the procedure.

4 Algorithmic Implementation and Complexity

We will briefly detail the main SDRG algorithm we have implemented for this report. Where necessary, we will add more details about how analyses were implemented as we reach them.

In studying disordered systems, we frequently need to take averages over disorder, i.e. many different realisations of the system in question. In many cases the number of trials must be very large for the required observables to converge - see [39] and [1] for examples of these issues. Thus an efficient and reliable algorithm is essential.

The key feature of our SDRG implementation is that it is almost totally memory static - that is, little or no extra memory is allocated in the computer every time a new disorder realisation is run. Rather, the existing memory used to hold data (e.g. bond strengths) is updated at the start of each realisation, and during the elimination process a 'mask' vector is maintained that tracks which bonds are active and should be used in calculation. The one off allocation of this mask vector is computationally very cheap compared to continually reallocating previous memory. An illustration of this approach can be seen in figure 4.1 and a psuedo-code version of our implementation can be seen in table 1.

Algorithm 1: SDRG step algorithm

Data: $\{J\}, L, \{(s_1, s_2)\}$
Result: $\{(s_1, s_2)\}$
$m \leftarrow 1$;
$active \leftarrow \{T\}^L$;
$n\_active = sum(active)$; `// will be used to track the number of active spins`
while $n\_active > 2$ **do**
  $J_M \leftarrow max\{(J_i\}$;
  $J_l \leftarrow J_{M-1}$;
  $J_r \leftarrow J_{M+1}$;
  $J' \leftarrow \frac{J_l J_l}{(1+\Delta)J_M}$;
  $J_l = J'$;
  $active_M \leftarrow F$;
  $active_{M+1} \leftarrow F$;
  $\{(s_1, s_2)\}_m \leftarrow \{(M, M+1)\}$;
  $m \mathrel{+}= 1$;
  $n\_active = sum(active)$;
end
$\{(s_1, s_2)\}_{L \div 2} \leftarrow \{(J_1, J_2)\}$;
return $\{(s_1, s_2)\}$;

To give an estimate of the efficiency of this procedure, we benchmarked the code for varying levels of machine precision and vary system lengths L. The results can be seen in figure 4.2. The elimination procedure for a system of $L = 1000$ spins is on the order of four microseconds. This implies that upwards of $200,000$ SDRG eliminations can be calculated in one second.

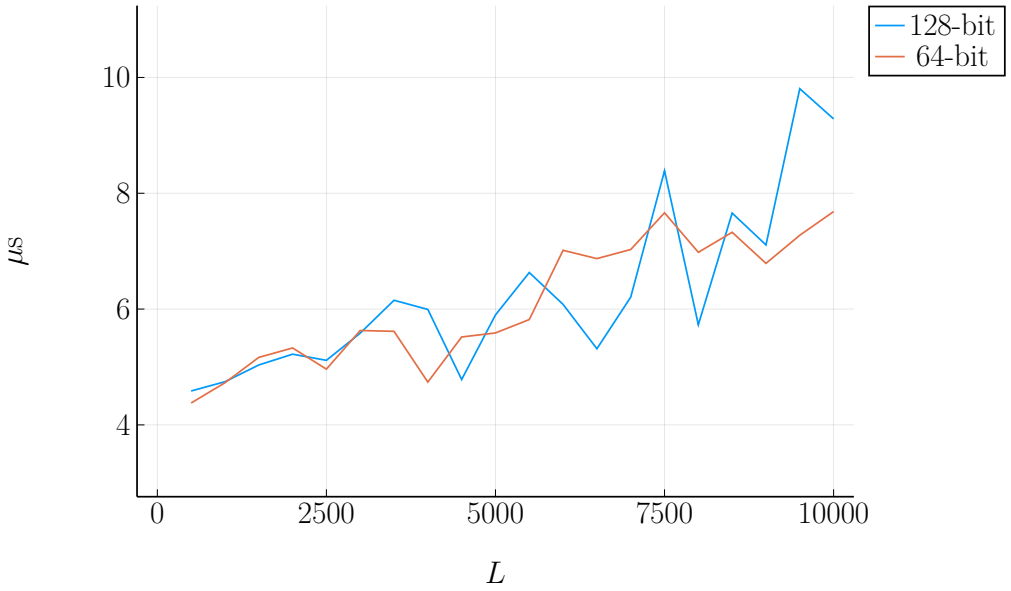

Figure 4.2: Benchmark results for our SDRG procedure. On the horizontal axis we measure the system length L, and on the vertical we report the median execution time for the complete SDRG procedure in microseconds. The execution time increases linearly in the system length for systems L in the order of thousands, and there is only a small performance penalty for using quadruple precision floating point numbers (i.e. 128 bits).

In practice, the analysis calculations slow down the 'rate of realisations' considerably. TO demonstrate this, we calculate the time taken to calculate the entanglement entropy S over a system of size L for $l \in [1, L \div 2]$ across N disorder realisations, at 64 and 128-bit accuracy within the SDRG procedure. Our results are shown in figure 4.3. In general we observe roughly linear scaling in both L and N. Calculating the entanglement entropy of a system of length 2000 across 2000 disorder realisations takes around 12 seconds, regardless of the floating point definition. This is well within acceptable for the immediate verification of results and could probably be improved upon considerably with refinements to the analysis code, and the refactoring of the code to work on distributed systems (e.g. industrial level high performance computerss (HPCs)).

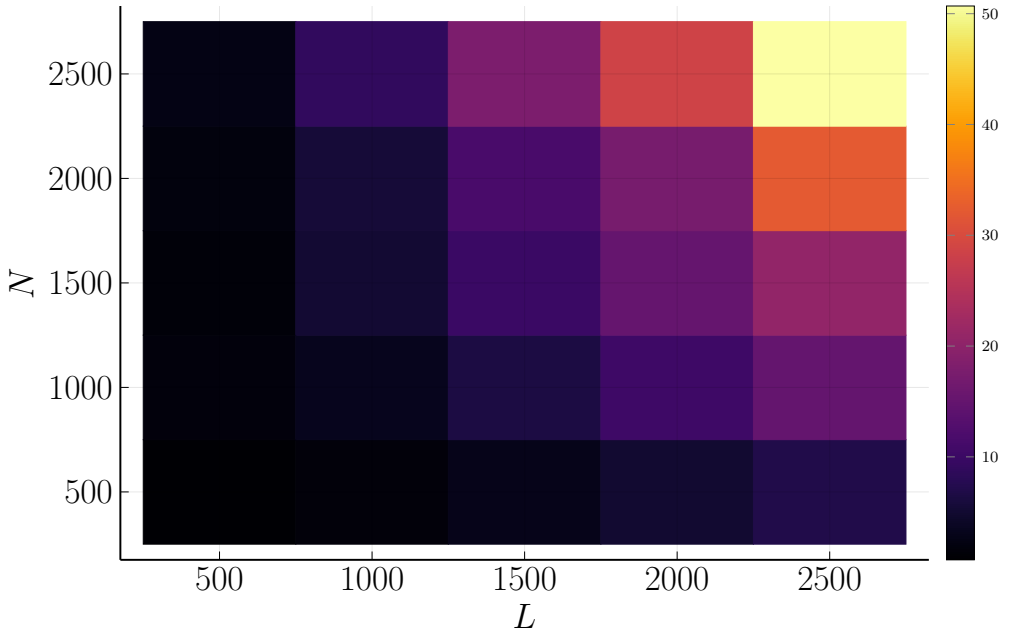

(a) Heatmap of the execution time in seconds to calculate the entanglement entropy S of system of length L for $l \in [1, L \div 2]$ across N disorder realisations at 64-bit accuracy. The colour represents the execution time in seconds.

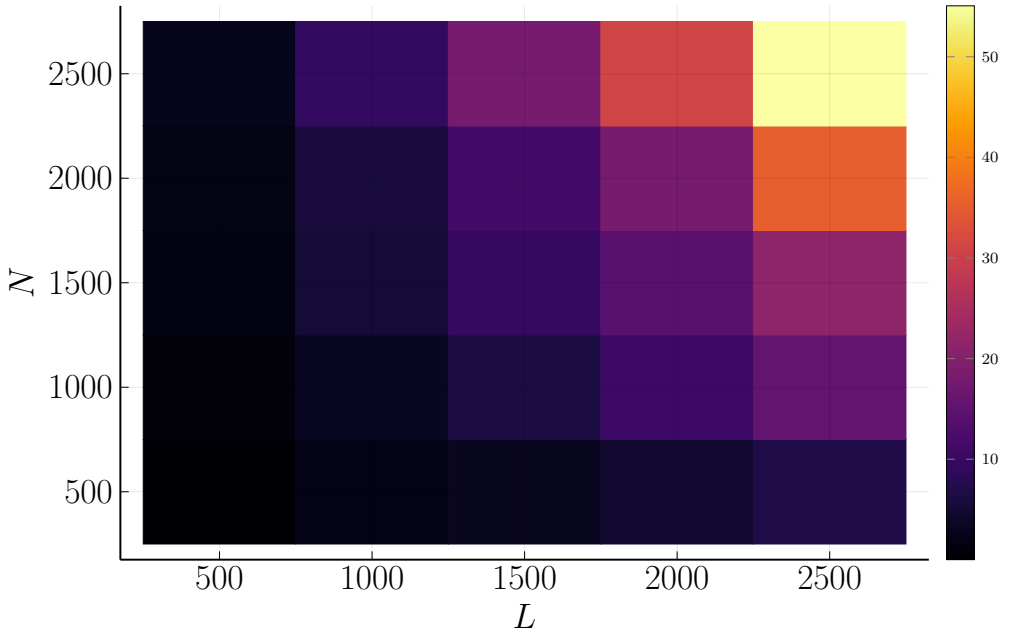

(b) Heatmap of the execution time in seconds to calculate the entanglement entropy S of system of length L for $l \in [1, L \div 2]$ across N disorder realisations at 128-bit accuracy. The colour represents the execution time in seconds.

Figure 4.3: Heatmap of the execution time in seconds to calculate the entanglement entropy S of system of length L for $l \in [1, L \div 2]$ across N disorder realisations at 64- and 128-bit accuracy. The colour represents the execution time in seconds. 4.3a: timings for 64-bit accuracy int he SDRG procedure. 4.3b: timings for 128-bit accuracy in the SDRG procedure.

5 Existing Results and Verification

A number of results for the scaling of entanglement measures already exist (see [7], [1], [2]). In this section we will reproduce these results and in the process, verify that the SDRG algorithm and related code works as expected.

5.1 Entanglement Entropy

As per [1], we measure the entanglement entropy of the disordered chain with and without periodic boundary conditions. The results are shown in figure 5.1. In this simulation we measure the entanglement entropy of a subsystem of length l located in the left hand side of the the XXX chain.

For each simulation, we draw L random couplings from the uniform distribution over $[0, 1]$ and run the SDRG algorithm (see 1). The SDRG algorithm returns a vector of tuples of sites, where each tuple represents a pair of spins. It is known from [7] that the ground state of the random spin chain (equation 3.1) is a *random singlet phase* (RSP), made up of $L \div 2$ singlets each entangled in a valence bond, e.g. a valence bond state. Each pair of singlets has the state given in equation 3.5. On this vector of singlet pairs we then run the relevant analysis. In the case of this entropy calculation, for every realisation of the RSP we measure the entanglement entropy (equation 1.1) for all window sizes l, and maintain a running mean of the result as a function of l.

We run the analysis for $L = 1000$ and $L = 2000$ for $50,000$ disorder realisations and in each case calculate from $l = 10$ to $l = L \div 2$ with an interval of 10 in between. For the periodic case (figures 5.1a and 5.1c) the finite size effects are smaller, and can be easily corrected with the following two mappings:

$$\ell \to L_c \equiv \frac{L}{\pi} Y\left(\frac{\pi \ell}{L}\right) \tag{5.1}$$

$$Y(x) = \sin(x)\left(1 + \frac{4}{3} k_1 \sin^2(x)\right) \tag{5.2}$$

where $k_1 = 0.115$, given by [40].

As can be seen in all four subfigures of figure 5.1, entropy scales logarithmically with the subsystem size. This is clearly an area law violation, and perfectly follows the prediction in [7]:

$$S_A = \frac{\ln 2}{3} \ln \ell + K \tag{5.3}$$

In the unadjusted l cases we notice that for large l the entropy begins to decrease again, as we would expect in a finite system. It should be noted that in figure 5.1c the degree of divergence from the log-linear trend is less than is seen in [1]. This is because we have chosen to calculate the entanglement entropy only up to $L \div 2$.

5.2 Logarithmic Negativity

In this section we recalculate the logarithmic negativity as reported in [1]. As we discussed in section 2, logarithmic negativity is in some sense a superior measure to the entanglement entropy because it is only measurable for pure states. As in [1], we calculate the logarithmic negativity of the one dimensional XXX chain (the same as in section 5.1). The pair of subsystems of length l is taken from the left hand side of the chain and extended in increments of 10 for every disorder realisation. The simulations are for the adjoint case, i.e. $r = 0$.

We run our analysis on systems of $L = 1000$ and $L = 2000$ for $50,000$ disorder realisations. We conducted the analysis in the OBC and PBC cases. The results can be seen in figure 5.2. In particular we have plotted the shifted negativity as defined in [1]:

$$\mathcal{E}^s_{A_1:A_2} = \mathcal{E}_{A_1:A_2} - \frac{\ln 2}{6} \ln L \tag{5.4}$$

Furthermore, we fit the predicted SDRG results for the periodic case to figure 5.2a:

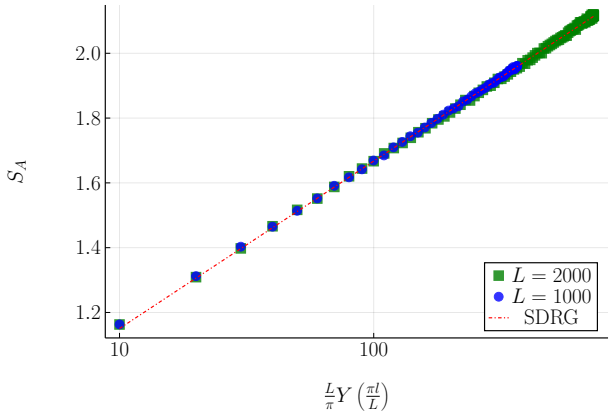

(a) Entanglement entropy of the XXX chain, adjusted l, PBC

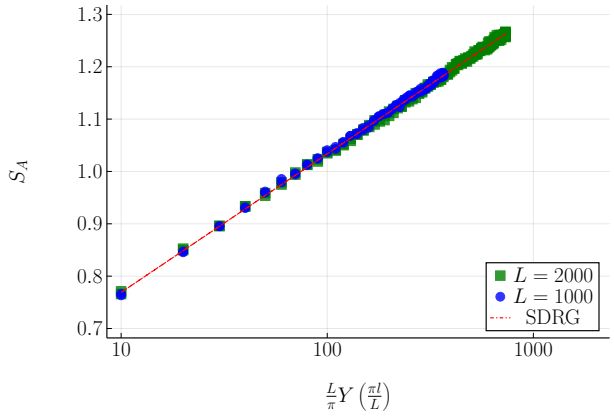

(b) Entanglement entropy of the XXX chain, adjusted l, OBC

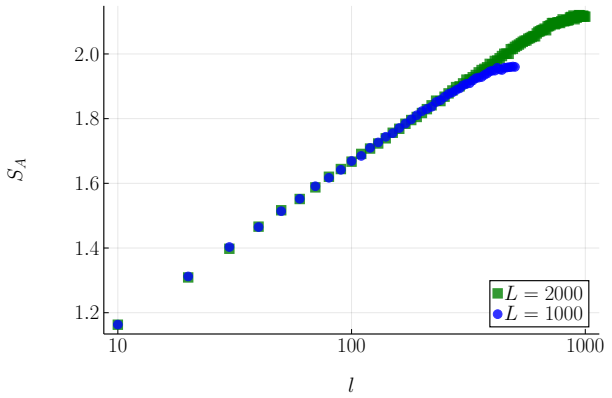

(c) Entanglement entropy of the XXX chain, no l adjustment, PBC

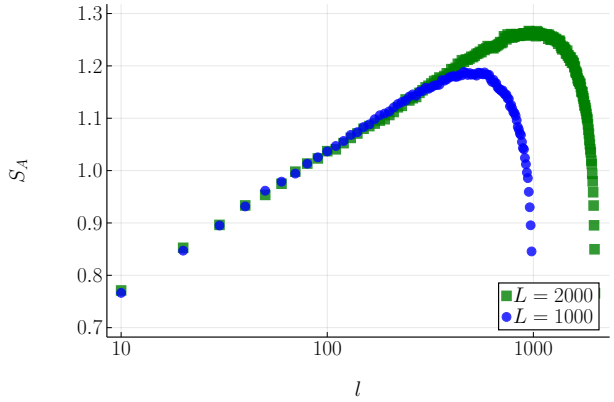

(d) Entanglement entropy of the XXX chain, no l adjustment, OBC

Figure 5.1: Entanglement entropy, recalculated from [1]. We measure the entanglement entropy of a subsystem of length l located in the left hand side of the the XXX chain. Each simulation is run for $50,000$ disorder realisations. 5.1a: the periodic chain with the adjusted subsystem length L_c. 5.1b: the open chain with the adjusted subsystem length L_c. 5.1c: the periodic chain with the unadjusted subsystem length l. 5.1d: the open chain with the unadjusted subsystem length l.

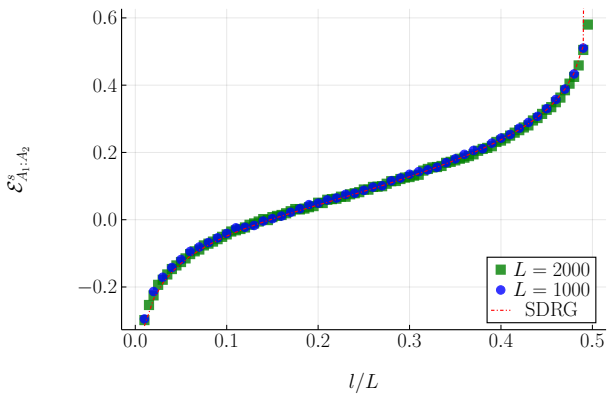

(a) Shifted logarithmic negativity as a function of l/L for the for XXX chain, $\delta = 1$, periodic boundary conditions.

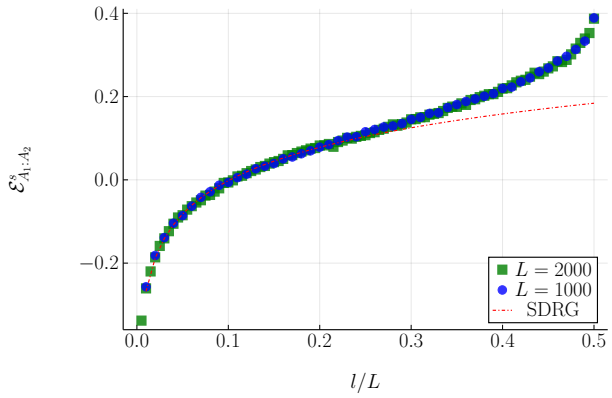

(b) Shifted logarithmic negativity as a function of l/L for the for XXX chain, $\delta = 1$, open boundary conditions.

Figure 5.2: Shifted logarithmic negativity, recalculated from [1]. In all figures, we measure the logarithmic negativity of two adjacent subsystems of length l located in the left hand side of the the XXX chain (i.e. $\Delta = 1$). Each simulation is run for 50,000 trials. For implementation details, see 5.2. 5.2a: shifted logarithmic negativity of the periodic chain with the subsystem length l. The fit is with equation 5.4. 5.2b: shifted logarithmic negativity of the open chain with the subsystem length l. The fit is with equation 5.6.

$$\mathcal{E}^s_{A_1:A_2} \simeq \frac{\ln 2}{6} \ln \frac{Y_c^2(\pi \ell/L)}{Y_c(2\pi \ell/L)} + k \tag{5.5}$$

which is a perfect fit for the periodic chain. For the open chain, we use the following identity from [1] for the logarithmic negativity in the case of an infinite chain:

$$\mathcal{E}_{A_1:A_2} = \frac{\ln 2}{6} \ln \left(\frac{\ell_1 \ell_2}{\ell_1 + \ell_2} \right) + k, \tag{5.6}$$

which is a good fit for $\ell/L << 1$.

In both cases (entanglement entropy and logarithmic negativity), it can be seen that the entanglement scales with a logarithmic correction to the area law for $l < L/2$. Beyond this point the finite size effects begin to dominate and we see the logarithmic negativity increase sharply, in line with what is reported in [2].

To summarise the preceding two sections, we have verified that for disordered models, both entanglement entropy and logarithmic negativity scale logarithmically. In the following section we will review the strongly inhomogeneous 'randbow chain'.

5.3 Randbow Chain

In this section we move on to reproducing the results of [2], which involves the modifying the couplings of the random chain to include an exponentially decaying term:

$$J_i \equiv K_i \times \begin{cases} e^{-h/2}, & i = 0 \\ e^{-h|i|}, & |i| > 0 \end{cases} \tag{5.7}$$

where the K_i terms are randomly distributed coefficients as before. This is known as the 'randbow chain'. The significance of these random couplings is to enforce a *rainbow* phase if the exponential parameter h is strong enough [8] - see figure 5.3 for an illustration.

For the $\lim h \to \infty$, the entanglement entropy of a subsystem A starting in the centre of the randbow chain (properly called the rainbow chain in this case) scales as a volume law. This is because for any subsystem l, the subsystem of size $l+1$ must contain another singlet link. For example, if our subsystem A starts as $A = \{J_1\}$, and then we extend it to $A = \{J_1, J_2\}$, these two subsystems have 1 and 2 singlet links in them respectively, and this holds for every other subsystem up to the maximum for $l = L \div 2$. Note that if we position the subsystem centrally in the chain, then the entanglement

entropy is always zero for the strong h phase as we only have 'complete singlets' in our subsystem (see [8] for an illustration, figure 2(b)).

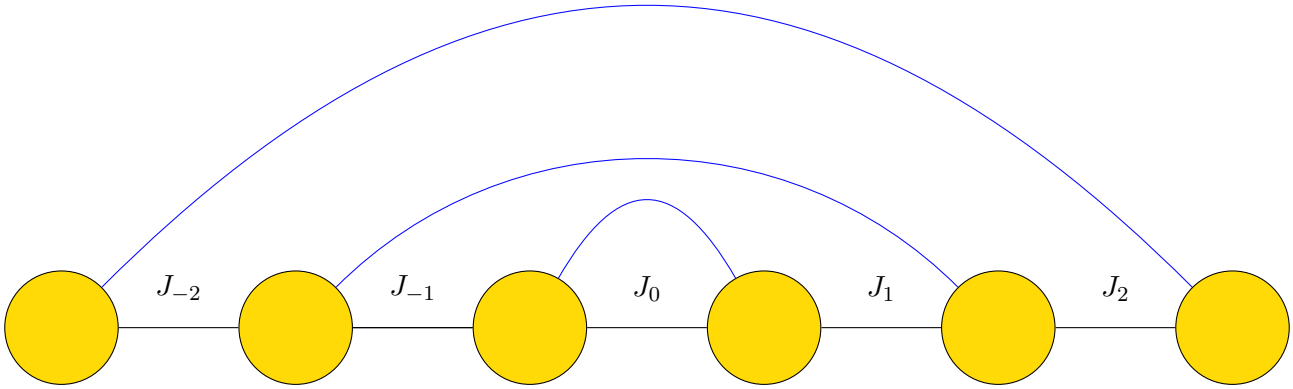

Figure 5.3: A rainbow chain as introduced in [8] and [2]. The central coupling J_0 is by definition the strongest coupling for the clean chain or for sufficiently large h, so it will always be eliminated first. The black edges represent the couplings $\{J_i\}$, whereas the blue edges represent the singlet links. Note that for the rainbow chain to make sense, we must have an odd number of links and an even number of spins in the open chain, hence the asymmetry in the diagram.

For the $h = 0$ phase we recover the random chain and the results from section 5.1 hold. However, for intermediate h we observe a square root correction to the area law [2]. This is presented in figures 5.4 and 5.5. As h increases, the scaling of the entropy gets closer to the volume law phase, as the effect of the 'rainbow' dominates. As we approach $h = 0$, the effect is weaker and we approach the random phase again. In 5.4 we measure the scaling of the entanglement entropy for a subsystem A of length l with its left edge on the centre of the chain. This positioning guarantees that we capture the volume scaling as h increases. We run both simulations for $50,000$ disorder realisations for the non-interacting open XX chain. We see clearly that a square root scaling holds, indicating a violation of the area law.

When we measure the entropy scaling for set ratios of h/δ, we observe a data collapse as first reported in [2]. The absolute values of h and δ no longer determine entanglement entropy but rather their ratio, with higher ratios leading to higher values of entanglement entropy. This is interestingly only the case of the SDRG procedure and does not hold in the exact solution for the XX chain (see section 5.5).

5.4 Randbow Subregion Analysis

To further verify the findings of [2] and to verify our own SDRG implementation, we recalculated specific elements of the contour analysis performed in that paper. Specifically, to understand the square root scaling we consider the probability densities of the sizes of the rainbow and 'bubble' regions. In any given realisation of the randbow chain, there will be subregions of continuous rainbow links and regions of continuous 'bubbles' (see figure 5.6 for an example).

We denote $P_r(l)$ the probability mass of seeing a rainbow subregion of length l, and similarly $P_b(l)$ for the probability of a bubble subregion of length l. We report these probability mass functions in figures 5.7a and 5.7b respectively, both with disorder parameter $\delta = 1$ and for a system size $L = 1000$ in the XX chain. We observe that for the rainbow distribution P_r, the probability of a region of length l decays exponentially in l, and that the rate of decay depends on h. However, for the P_b distribution, we observe a much slower power law decay, implying that there is no characteristic size of a bubble region, and furthermore that this does not depend on h at a scale visible on the plot.

This leads to an argument that the scaling of the entanglement entropy scales as a square root. We presented the following argument, adapted slightly from that given in [2]. Firstly, we observe from figure 5.7b that $P_b(l) = l^{-3/2}$, and thus:

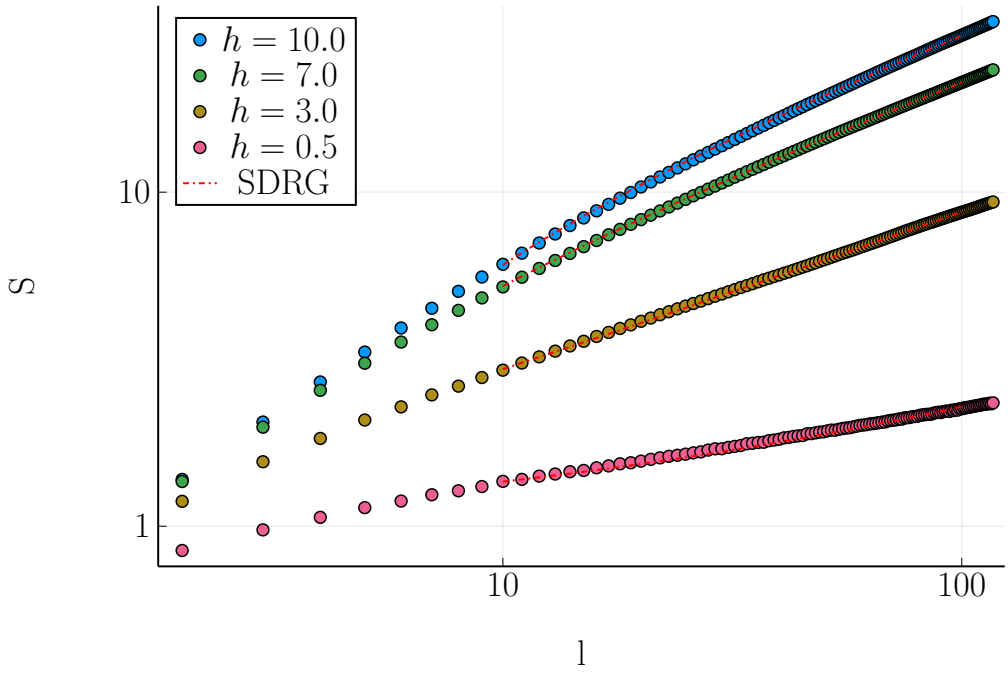

Figure 5.4: Entanglement entropy for the open XX randbow chain whilst varying the exponential parameter h. Notice the log-log scaling on each axis. Each simulation is run for 50,000 disorder realisations, and we measure the entanglement entropy of a subsystem A starting at the chain centre (offset by one to ensure the proper scaling) for each realisation. A fitted function of the form $y = a + b\sqrt{x}$ is overlayed for each value of h.

$$\langle l_b \rangle = \int_2^l dl l P_b(l) \propto l^{1/2} \tag{5.8}$$

Secondly, calling a 'bubble region' a subsystem of consecutive bubbles, and similarly a 'rainbow region', we notice that, very roughly, the number of bubble regions N_b must be equal to the number of rainbow regions N_r. Furthermore, dividing the total subsystem length l by the average length of a bubble region $\langle l_b \rangle$ gives N_b, and thus:

$$\frac{l}{\langle l_b \rangle} \propto N_b = N_r \tag{5.9}$$

The entanglement entropy is equal to the number of rainbow links in the subsystem multiplied by $\ln 2$, which is equal to the number of rainbow regions multiplied by the average length of a rainbow region:

$$S_A \propto N_r \times \langle l_r \rangle \times \ln 2 \tag{5.10}$$

Bringing together equations 5.9 and 5.10, we get:

$$S_A \propto \frac{l}{\langle l_b \rangle} \times \langle l_r \rangle \times \ln 2 \propto l^{1/2} \langle l_r \rangle \ln 2 \tag{5.11}$$

which suggests the observed square root scaling.

5.5 Randbow Chain Exact Solution

Finally, we analyse the exact solution of the XX chain. This is done by forming a matrix $C_{ij} = \langle c_i^\dagger c_j \rangle$ and taking a subset A of these matrix entries - this forms the reduced density matrix with respect to the A subsystem, from which we can calculate the entanglement entropy trivially. For a detail derivation, see section A.3.

In the following simulations, we calculate the exact solution to the XX randbow chain for a system with $L = 100$ spins. We take an average over 1000 disorder realisations for each disordered system

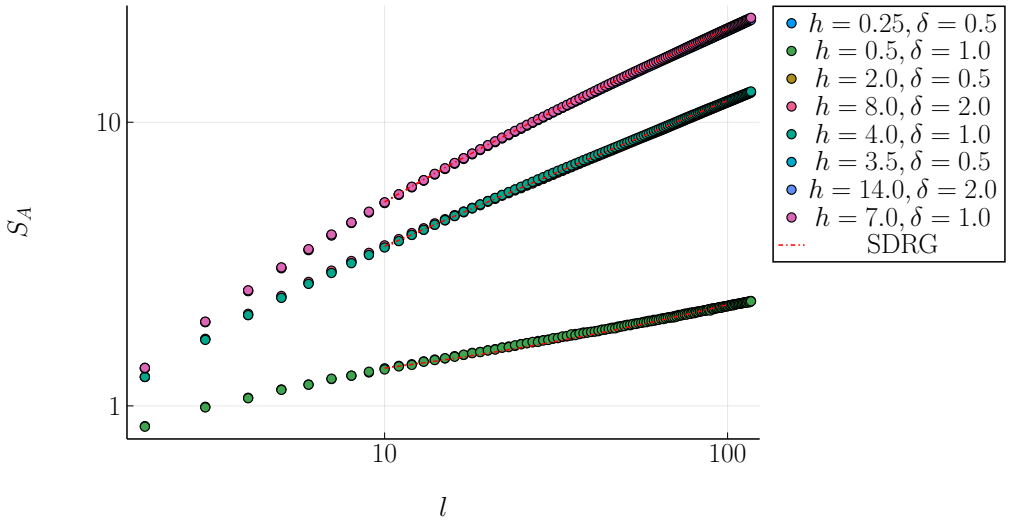

Figure 5.5: Entanglement entropy for the open XX randbow chain whilst varying the exponential parameter h and the disorder parameter δ in fixed ratios. Again, notice the log-log scaling on each axis. Each simulation is run for $50,000$ disorder realisations, and we measure the entanglement entropy of a subsystem A starting at the chain centre (offset by one to ensure the proper scaling) for each realisation. A fitted function of the form $y = a + b\sqrt{x}$ is overlayed for each value of h/δ.

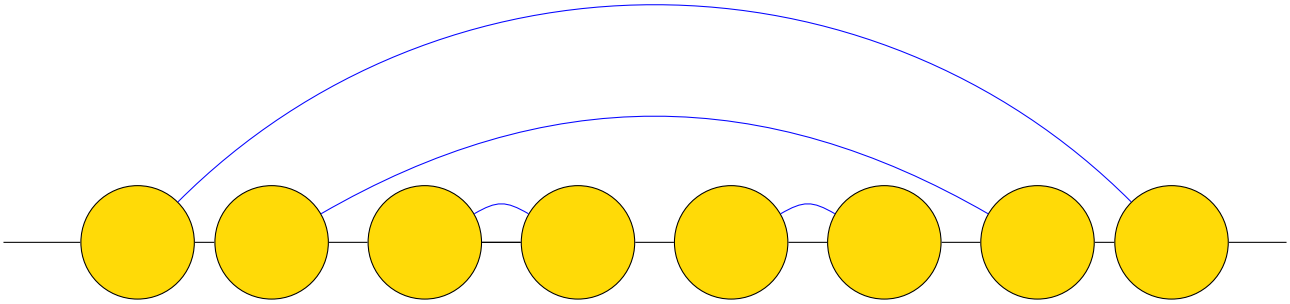

Figure 5.6: A demonstration of the bubble and rainbow subregions as named in [2]. The first two spins represent a randbow region of $l = 2$, and the second four spins represent a bubble region of $l = 4$.

and calculate the entanglement entropy from $l = 1$ to $l = 32$ for each realisation. For accuracy these simulations were run with 128-bit floating point numbers, which slows down the computation significantly as most optimised linear algebra routines are designed for 64-bit precision or lower. The results for the disordered cases are shown in figure 5.8a. Note the $\log_2$ scaling on each axis. The entanglement entropy retains its clear square root scaling, but we observe the the data collapse onto the h/δ ratios is no longer present. Furthermore, the absolute increase in h does increase the entanglement entropy at all scales l.

Furthermore, we calculate the entanglement entropy of the clean rainbow chain, and our results are in figure 5.8b. Here we have a logarithmic scale only on the y-axis and we see the volume law very clearly for all subsystems lengths l. This holds even for relatively weak inhomogeneity $h = 1.5$.

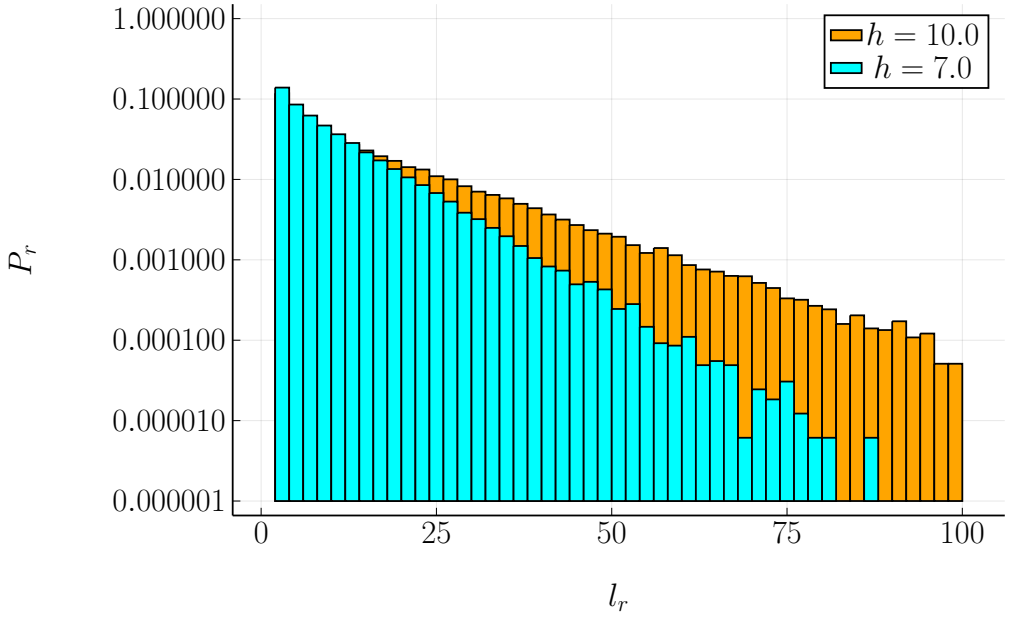

(a) Probability density function $P_r(l)$ of the lengths of rainbow subsystems. The data were collected by averaging over $10,000$ disorder realisations for $h = 10$ and $h = 7$ in the open XX chain, solved with the SDRG method. Notice the logarithmic scale on the y-axis only, suggesting an exponential decay.

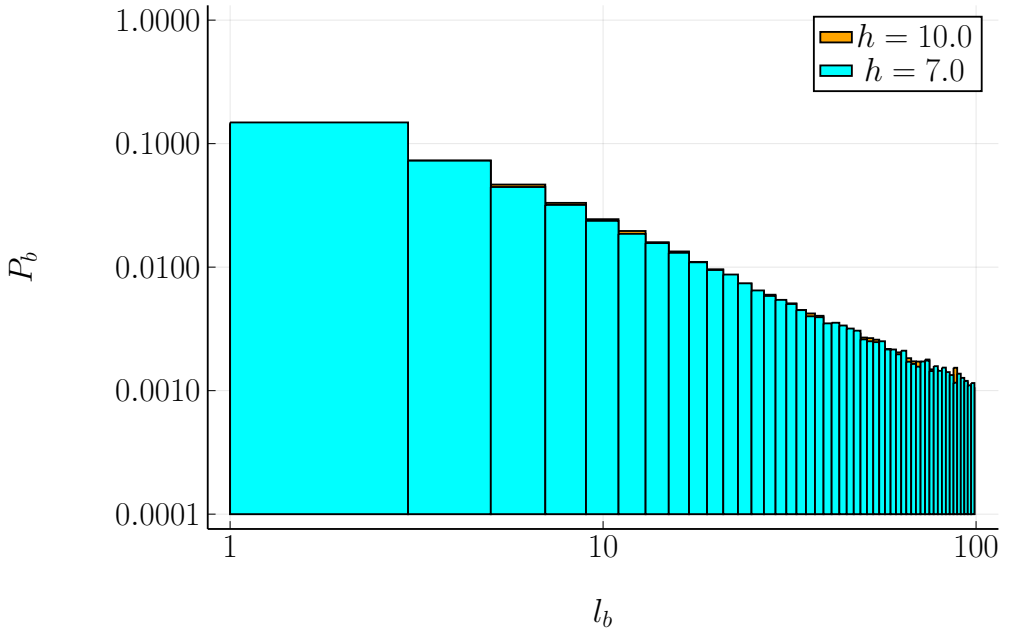

(b) Probability density function $P_b(l)$ of the lengths of bubble subsystems. The data were collected by averaging over $10,000$ disorder realisations for $h = 10$ and $h = 7$ in the open XX chain, solved with the SDRG method. Notice the logarithmic scale on both axes, suggesting a power law decay.

Figure 5.7: Subregion analysis for the XX chain of $L = 1000$. 5.7a: probability mass for rainbow region lengths. 5.7b: probability mass for bubble region lengths.

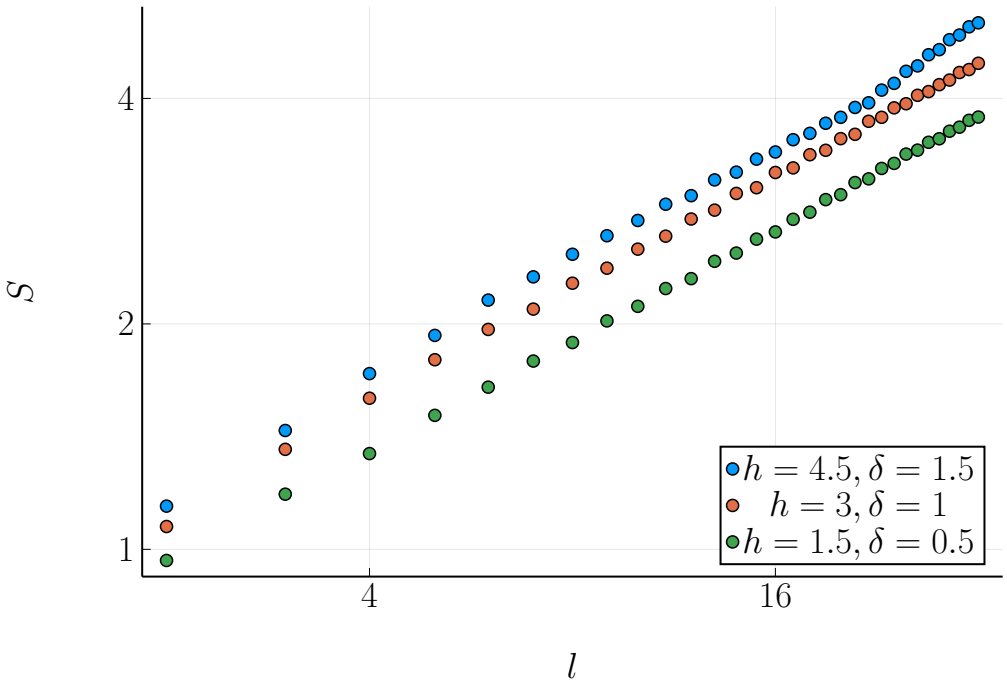

(a) Entanglement entropy scaling of the XX randbow chain with the exact solution. We calculate the solution for the $L = 100$ chain with $\delta = 1$ for $1,000$ disorder realisations. Notice the log-log scales. Notice that the data collapse on the ratio h/δ is no longer present.

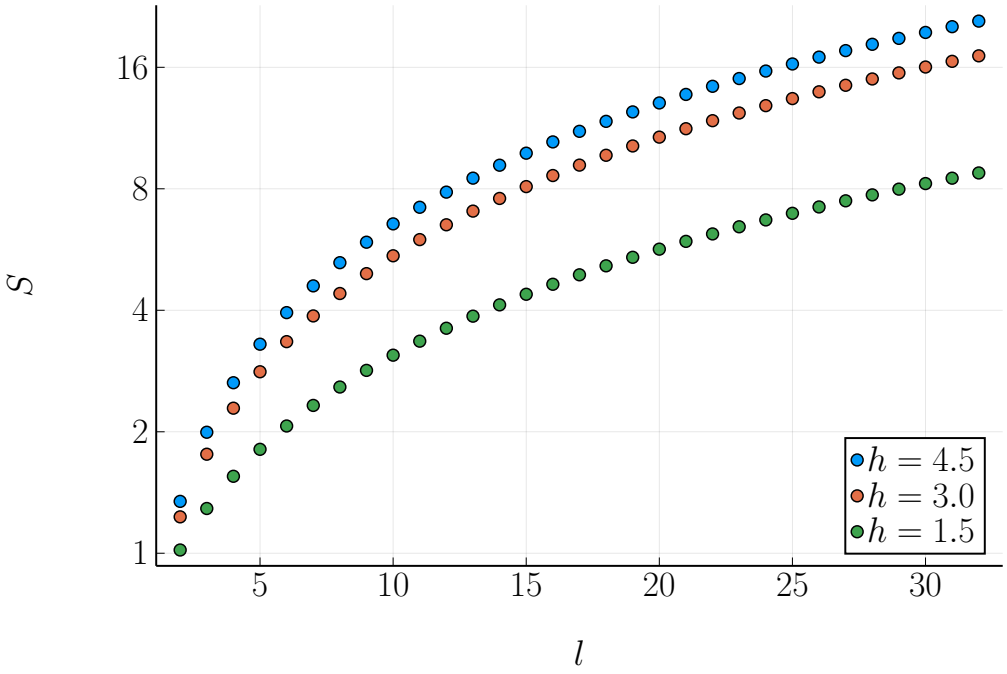

(b) Scaling of the entanglement entropy of the clean open XX chain, calculated with the exact solution to the groundstate problem with varying h. We use 1 trial for each value of h on a system of size $L = 100$, with $\delta = 0$. Notice the volume scaling in l and the logarithmic scaling only on the y-axis.

Figure 5.8: Entanglement entropy scaling of the randbow chain with the exact solution. We calculate the solution for the $L = 100$ chain. 5.8a: the exact solutions for the XX chain with disorder ($\delta = 1$) for $1,000$ disorder realisations. Figure 5.8b: the exact solution of the clean case.

6 Entanglement negativity for the randbow chain

6.1 Analytical expectation

In the following sections, we being our extension of the existing results. We start by analysing the logarithmic negativity we expect for an open randbow chain with two adjacent intervals as we vary the subsystem length l. This simulation setup is identical to that seen in 1.2, except that we use the randbow couplings rather than the basic disordered couplings.

For the $h \to \infty$ limit, we would expect the negativity to follow the volume law. The argument is essentially the same as that made for the large h entanglement entropy: for every extra $l + 1$, we introduce another singlet link between A_1 and A_2, thus we get a volume law.

For moderate values of h, we can predict a square root scaling via a very similar argument to that presented in 5.4. First, recall that the logarithmic negativity is simply the number of singlet links between the two subsystems, multiplied by $\ln 2$. Secondly, we assume that for moderate h, the groundstate of the SDRG procedure is symmetric with respect to the chain centre. This is reasonable for moderate h and is supported by further arguments with respect to the flow of eliminations presented in [2].

This allows us to consider just one of the two A subsystems (as we know that the other will be identical expect for a reflection in the indices i). Any rainbow links emerging from the subsystem A_2 will be going to the subsystem A_1 and vice versa [2], and thus will contribute to the logarithmic negativity. To understand the scaling of the logarithmic negativity, then, we only need to understand the scaling of the entanglement entropy of the subsystem A_2, which we know to be a square root scaling.

It is important to point out that this argument, based on that given in [2], only holds in the non-interacting case. We will see in the numerical evidence that that is indeed the case and the interacting model shows a saturating behaviour consistent with [2].

6.2 SDRG results

We measure the logarithmic negativity of two adjoint subsystems in the XX and XXX randbow chains, with $L = 1000$ and 2000 in both cases. We use the SDRG procedure for $50,000$ disorder realisations each, and plot the regular (i.e. not shifted as per 5.2) logarithmic negativity as a function of the adjusted subsystem length l/L. In both cases we use the parameters $h = 1, \delta = 1$ for the moderate inhomogeneity regime. Our results are shown in figure 6.1.

As can be seen from figure 6.1a, in the XX case the square root scaling is captured perfectly. Furthermore, for larger values of l we notice that the logarithmic negativity is higher for a given fraction of the chain. This is to be expected: for a longer chain, there will be more singlet links in a subsystem for length $0.5L$, etc.

In the XXX model, we observe the same saturation behaviour reported for the entanglement entropy in [2]. This is to be expected given the the argument made above in section 6.1: to calculate the logarithmic negativity we only need to know the entanglement entropy, and we already expect this to saturate in l.

It is interesting to note that the saturation implies an area law regime, and to consider why this occurs only in the interacting case. It is argued in [2] that the bubble regions in the interacting model are much more stable, which invalidates the heuristic argument presented for the square root scaling and leads to a saturation, because there is not enough space in the subsystem for rainbow links. The details of this argument are beyond the scope of this report but are covered in more detail in [2].

As an additional measure of the rate at which entanglement decays from the centre of the chain, we measure the logarithmic negativity as we vary the interval r between two adjacent intervals in the XX and XXX chains. We consider only even r, with the interval spaced evenly over the centre of the chain (see figure 1.2 for a visualisation) with $L = 1000$. We observe that the in the XX case, the logarithmic negativity decays relatively slowly as r increases. This is to be expected given the

[2] We ignore the possibility that a rainbow link could leave A_2 'to the right' and attach to the remainder of the chain. It is shown in [2] that this is a very accurate approximate from moderate h.

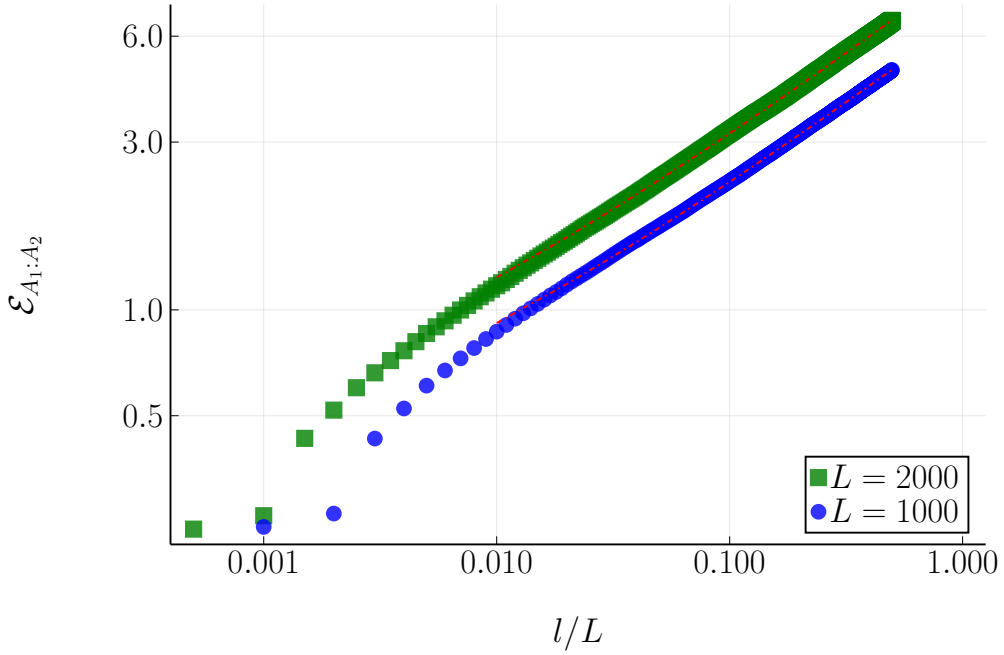

(a) Logarithmic negativity for the open randbow XX chain. Notice the logarithmic scale on both axes. The fitted curve is of the form $a + b\sqrt{x}$.

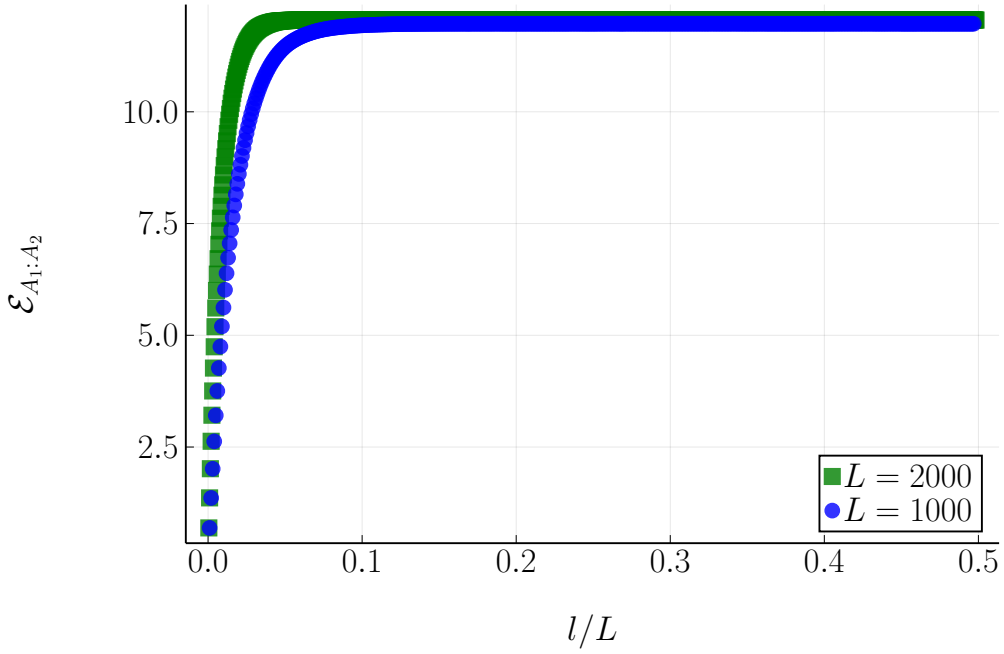

(b) Logarithmic negativity for the open randbow XXX chain. Notice the rapid saturation, indicative of an area law.

Figure 6.1: Logarithmic negativity scaling in the open randbow chain for adjoint subsystems. We set $h = 1, \delta = 1, L = 100$ in both figures and measure the logarithmic negativity over $50,000$ disorder realisations. We place the subsystems A_1 and A_2 in the centre of the chain, i.e. with the right hand edge of A_1 next to the left hand edge of A_2. In both figures we run the simulation for $L = 1000$ and $L = 2000$. 6.1a: scaling in the XX regime. A square root scaling is observed, reflecting analytical expectations and the results from 5.5. 6.1b: scaling in the XXX regime. We observe that the logarithmic negativity saturates quickly in both system lengths.

previously discussed stability of the rainbow regions in the XX case relative to the bubble regions. Furthermore, we notice a strong data collapse onto the ratios h/δ, just as for the previous measures of entanglement.

However, in the interacting XXX case, the logarithmic negativity decays far more quickly, as expected from the saturating behaviour we see in figure 6.1b. This is a corollary of figure 6.1b: as we extend further into the extremes of the chain, the entanglement is generally local and we lose long distance information.

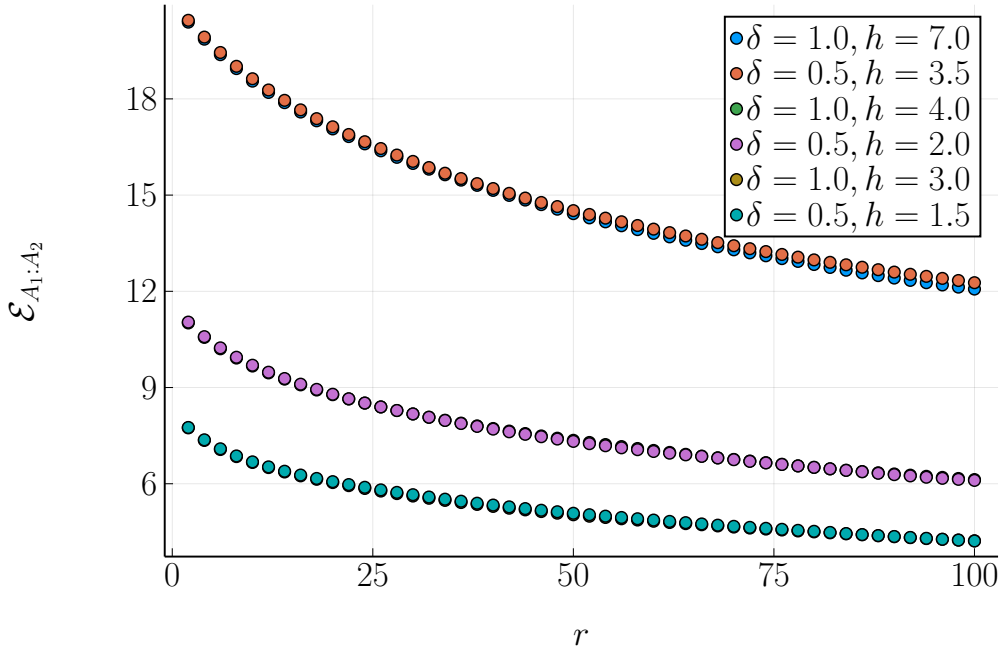

(a) Randbow central negativity with varied r, XX, OBC

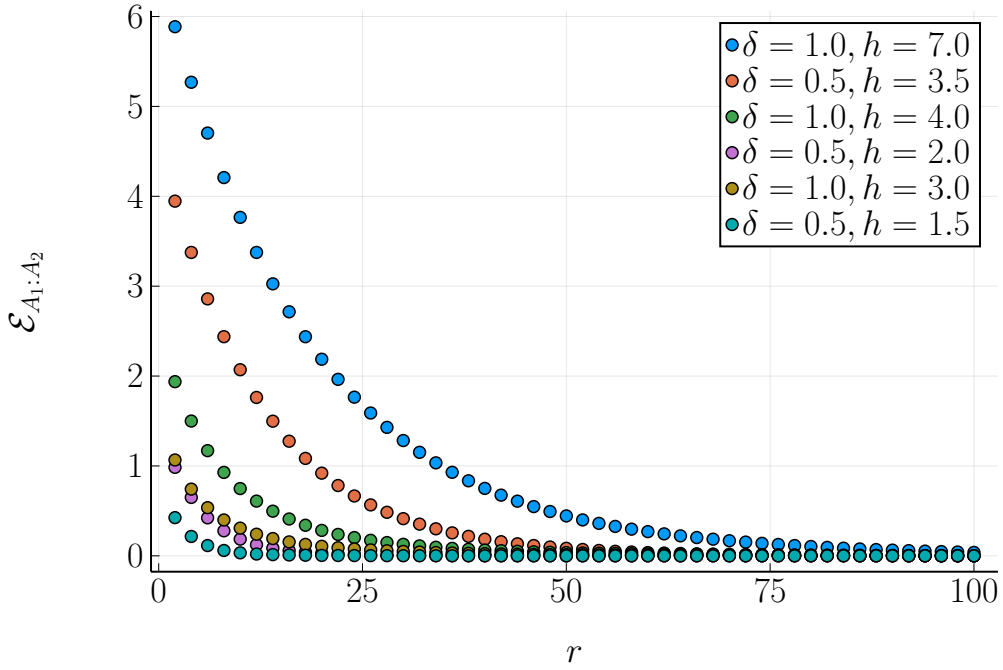

(b) Randbow central negativity with varied r, XX, OBC

Figure 6.2: Logarithmic negativity scaling in the open randbow chain for disjoint subsystems as we vary r. We measure the logarithmic negativity over $50,000$ disorder realisations. We place the subsystems A_1 and A_2 in the centre of the chain separeted by an even interval r, located in the centre of the chain. $L = 1000$ and $l = 100$ in both figures. 6.2a: the XX chain. The logarithmic negativity decays relatively slowly, in line with figure 6.1a. We also observe a strong data collapse onto the ratio h/δ. 6.2b: scaling in the XXX regime, $\Delta = 1$. The logarithmic negativity decays much more quickly, in line with figure 6.1b, and there is no observable data collapse other than the $r \to 0$ limit in which all entanglement is lost.

7 Power law systems

In [8], it is mentioned that the couplings must decay relatively quickly in order for the complete rainbow chain to be enforced. In particular they suggest that:

$$J_i = \mathcal{E}^{\alpha(i)} \tag{7.1}$$

where $\alpha(i)$ is monotonically decreasing. To explore how sensitive the scaling of entanglement is to the speed of this decay, we consider a new power-law system with couplings given by:

$$J_i \equiv K_i \times \begin{cases} 2, & i = 0 \\ |i|^{-\alpha}, & |i| > 0 \end{cases} \tag{7.2}$$

In the case were $i = 0$, i.e. when we are determining the central coupling, we have chosen 2 as the second factor to ensure that the total function $F(i)$ (see 3.2) is peaked at i.

In the follow sections, we discuss the analytic expectations for the scaling of the entanglement entropy and the logarithmic negativity in the case of the power-law couplings.

7.1 Power law systems: analytical expectations

In [2], it is possible to derive analytical expectations for the randbow chain only in the strong inhomogeneous limit $h \to \infty$ (see in particular section VI.A). This is because only in the inhomogeneous limit (and with symmetric J_i) can we be sure the the central bond will always be eliminated first and that the elimination process will be symmetric with respect to the chain.

Unfortunately, for the power-law system, we cannot guarantee that the central bond will be eliminated first, nor that the process with be symmetric. The reason is that the effect of the power-law component is not enough, relative to the effect of the $\mathcal{O}(1)$ disorder factor, to rapidly reduce the consecutive couplings. Given that, as discussed in section 3.3, the elimination rule always reduces the energy scale, the couplings around the elimination site must be small enough to still be smaller than the new J' coupling. In the power-law system, this cannot be guaranteed to be the case.

Therefore we cannot make any rigorous predictions about the entanglement scaling for the power-law system. However, given that we do not expect the couplings to decay quickly enough to maintain a rainbow phase, we might expect that the power-law system will behave at least asymptotically as the simple disordered system. Thus we can make the following general hypotheses:

1. The entanglement entropy will scale in a manner similar to the simple disordered spin chain as seen in section 5.1.

2. The logarithmic negativity will also scale in a manner similar to the simple disordered spin chain as seen in section 5.2.

We will explore these results within the SDRG framework and with the exact solution.

7.2 Entanglement Entropy: SDRG and exact results

We start by calculating the scaling of the entanglement entropy of the open XX power-law chain with $L = 1000$ and $L = 2000$. We use $\delta = 1$ in all of our simulations and position the subsystem A with the left hand edge on the centre of the chain, to properly capture the scaling as in the randbow simulation (see 5.3). We run all of the simulations for $50,000$ disorder realisations and the results are shown in figure 7.1.

In both figures, we can see that, as expected, the entanglement entropy scales similarly to the simple disordered model. For very low l we notice that the entanglement scales very quickly, which suggests that the rainbow phase does survive for at least the first few eliminations on average. After the initial phase, the scaling becomes quasi-logarithmic, confirming the hypothesis in section 7.1. Furthermore, we notice that for larger values of α, the entanglement entropy is generally larger. This accords with our intuition that for stronger inhomogeneity, the rainbow regions should be more stable

and they are the regions that contribute to the entanglement entropy. Lastly, we observe some finite size effects for $l/L \approx 1/2$. We have not attempted to fit any of the analytical curves from the simple disordered model due to the very different low l region.

To determine whether it was possible to force a volume law scaling in the power-law model, we calculated entanglement entropy for the $L = 2000$ XX chain for very high values of α. Our results are shown in figure **??**. We observe that as α becomes larger, the scaling of the entanglement entropy does become linear but with a coefficient much lower than would be expected for a rainbow phase. For example, in a subsystem of length 750 we would expect an entanglement entropy of $\ln 2 * 10 \approx 500$, but instead we see an entanglement entropy of 1.5 when $\alpha = 500$ and $l = 750$. This suggests that we still do not well understand this power-law system.

Furthermore, we measure the entanglement entropy via the exact solution. Over 1000 disorder realisations, we measure the scaling of the entanglement entropy of the XX power-law chain for an open chain of length 100. Our results are shown in figure 7.3. Once again, the scaling of the entropy is logarithmic (notice the log-log scaling) and this matches the general scaling pattern observed in figures 7.1a and 7.1b. Interestingly, we observe a strong data collapse onto the ration α/δ.

7.3 Logarithmic negativity scaling

In this section, we look at the logarithmic negativity of the power-law system. Specifically we measure the logarithmic negativity of the open XX and XXX power-law chains for $L = 1000$ and $L = 2000$. We run each simulation for $50,000$ disorder realisations, and our results are shown in 7.4.

For both values of L, we observe that the scaling is identical to that of the simple disordered chain. This confirms our earlier hypotheis about the power-law systems. Interestingly, the curve for $L = 2000$ is higher in both the XX and the XXX simulations than the $L = 1000$ curve. This is best explained by the presence of some persistent rainbow regions even in the power-law model: in terms of absolute logarithmic negativity, half of the $L = 2000$ rainbow chain will contain more singlet links between the two subsystems than the equivalent subsystem of a relative size for $L = 1000$.

Finally, we calculate the scaling of the logarithmic negativity for a varying interval r between two subsystems, in a manner identical to that discussed in 6.2. Our results for the open XX and XXX chains with disorder $\delta = 1$ are reported in figure 7.5. We observe that, much like the interacting randbow chain, the logarithmic negativity decays much more quickly than in the randbow chain, which we would expected given the relative instability of the rainbow regions.

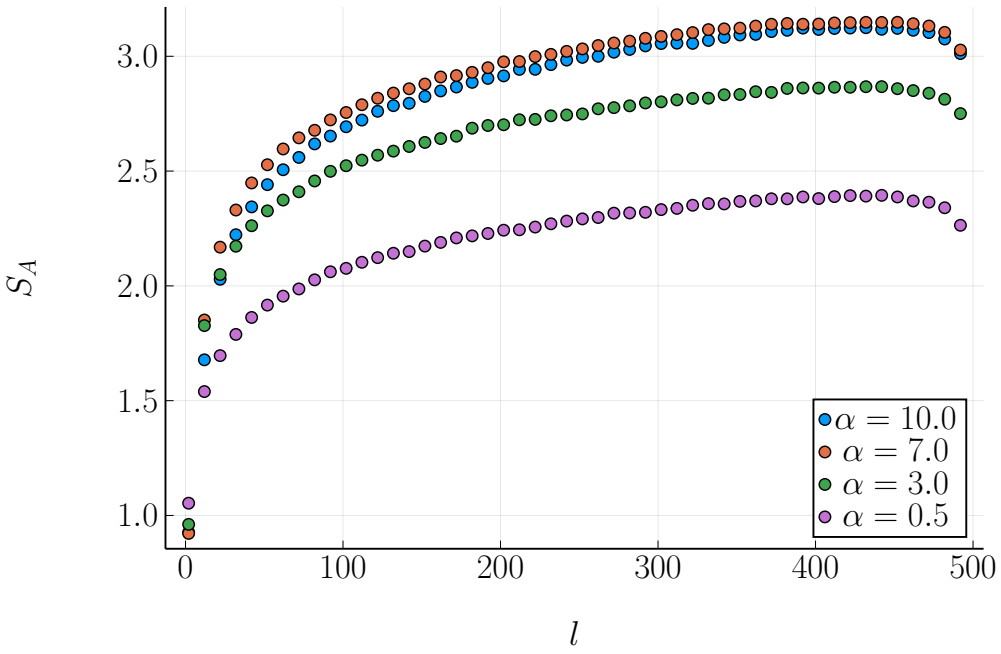

(a) Powerbow entropy via SDRG, $L = 1000$, varying α, OBC

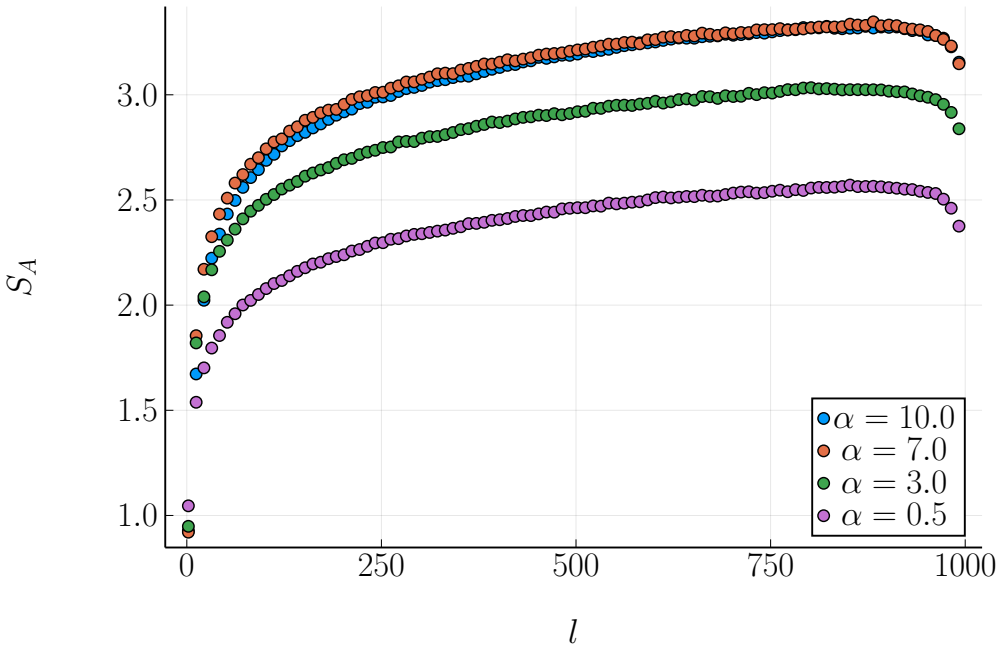

(b) Powerbow entropy via SDRG, $L = 2000$, varying α, OBC

Figure 7.1: Entanglement entropy for the open XX power-law system, calculated via the SDRG method. We $L = 1000$ and 2000. In both figures, we calculated the entropy of a subsystem A with the left edge on the centre of the chain to capture the proper scaling over $50,000$ disorder reaslisations. For each system size we ran the simulation with a different parameter α as per equation 7.2. Figure 7.1a: $L = 1000$. Figure 7.1b: $L = 2000$.

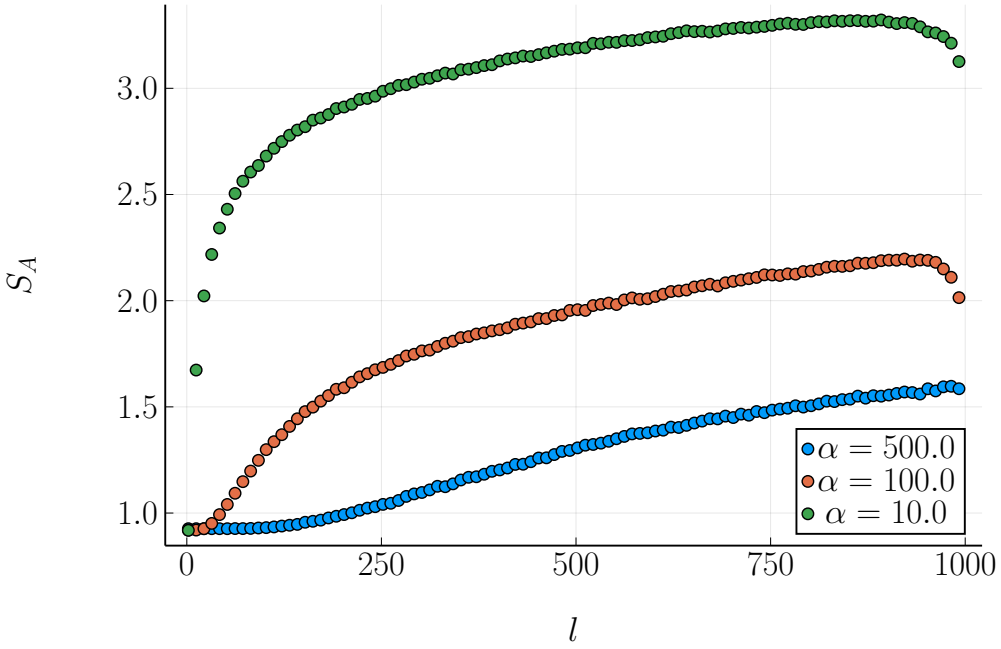

Figure 7.2: Entanglement entropy of the strong inhomogeneous limit of the open XX power-law system, calculated with the SDRG method over $50,000$ disorder realisations with $\delta = 1$. For each simulation we vary the α. The system length is $L = 2000$. Notice the more linear but lower entanglement entropy for high α.

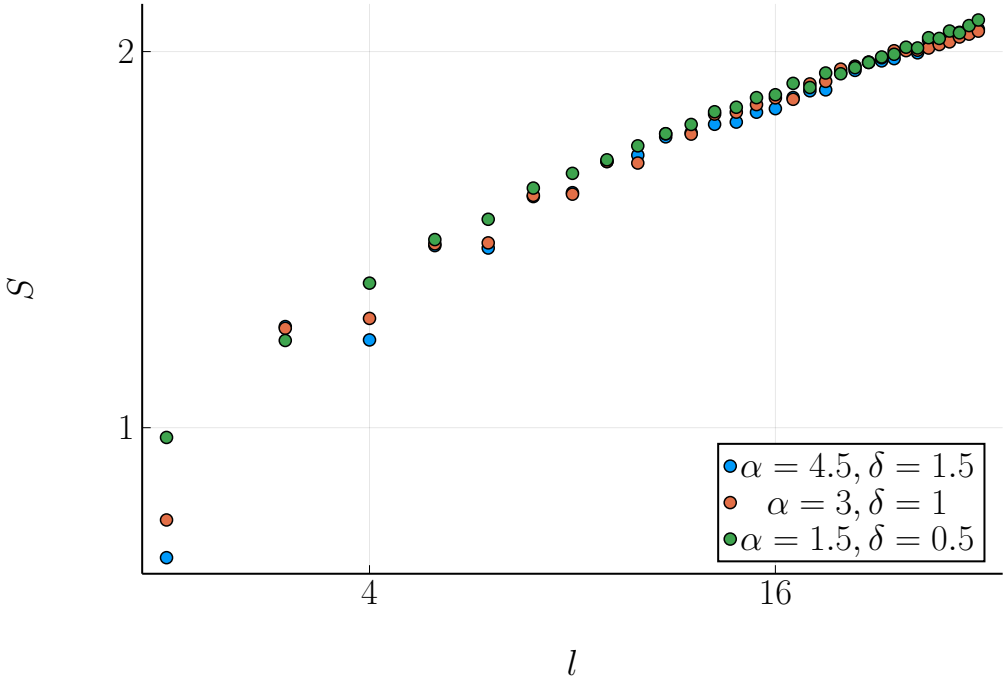

Figure 7.3: Entanglement entropy of the open XX power-law system, calculated with the exact solution over $1,000$ disorder realisations with $\delta = 1$. For each simulation we vary the α. The system length is $L = 100$. Notice the log-log scale.

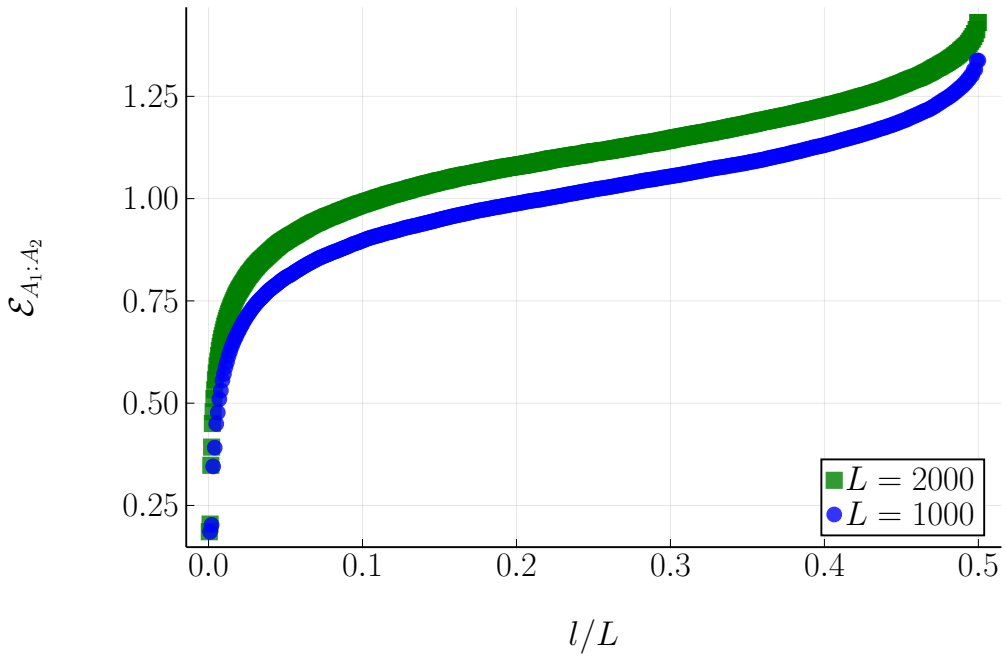

(a) Scaling of the logarithmic negativity, XX, OBC

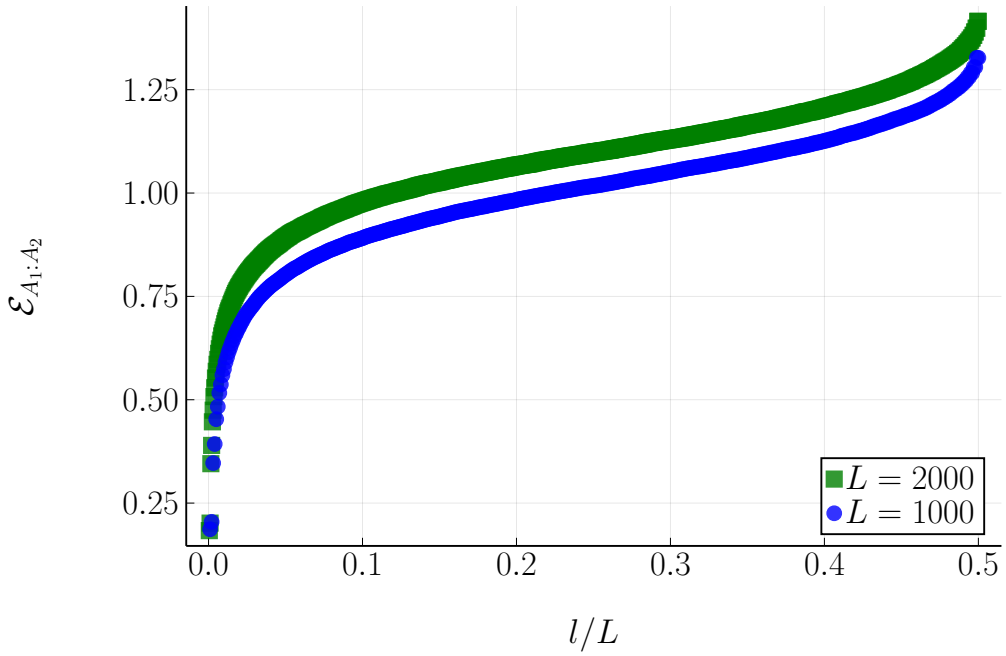

(b) Scaling of the logarithmic negativity, XXX ($\Delta = 1$), OBC

Figure 7.4: Scaling of the logarithmic negativity of the open power-law system. In each figure we calculate the negativity over $50,000$ disorder realisations whilst keeping $\alpha = 1, \delta = 1$. Figure 7.4a: logarithmic negativity for the XX chain. Figure 7.4b: logarithmic negativity for the XXX $\Delta = 1$ chain. Notice that in each subfigure, the $L = 2000$ curve is shifted upwards relative to the $L = 1000$ curve.

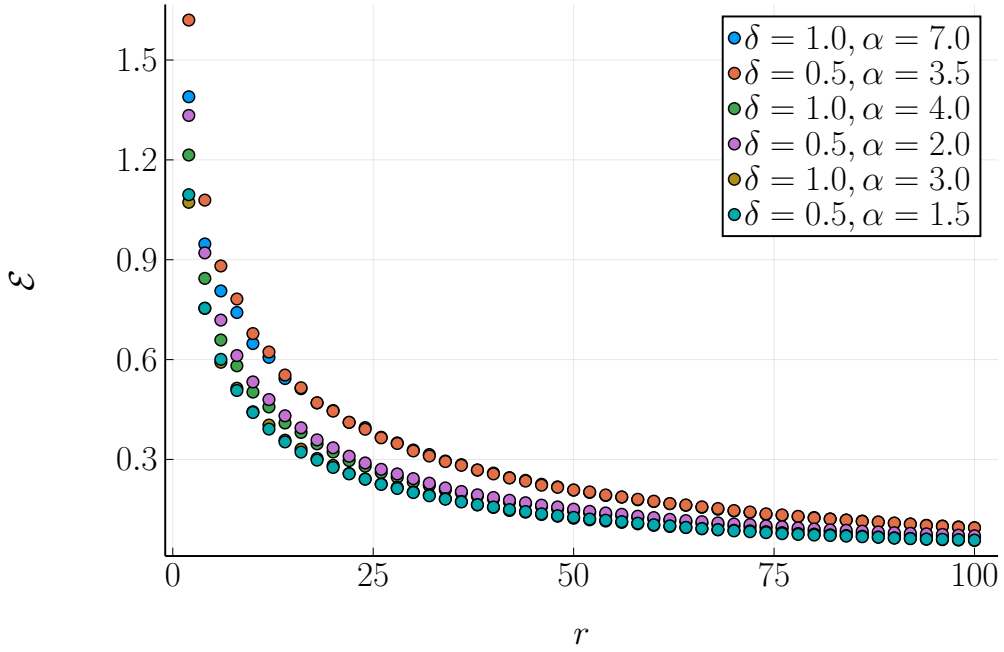

(a) Logarithmic negativity with varying r, XX, OBC. Notice in this case that there is a data collapse for small r onto the ratio α/δ.

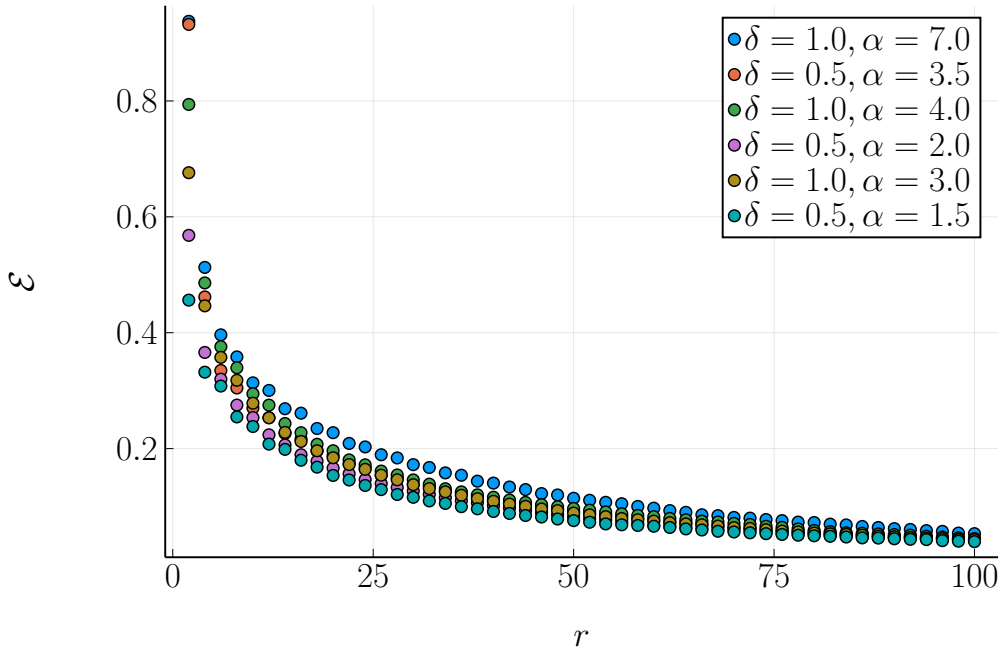

(b) Logarithmic negativity with varying r, XXX ($\Delta = 1$), OBC. Notice in this case that there is no obvious data collapse for small r.

Figure 7.5: Scaling of the logarithmic negativity of the open XX and XXX power-law systems as r is varied. We restrict r to even intervals and the position is the same as per figure 6.2. $L = 1000$ and $l = 100$ in both figures. We notice that the logarithmic negativity decays very quickly compared to the non-interacting randbow case, figure 6.2a.

8 Conclusion

In this report we have confirmed some key findings in the literature on entanglement scaling in random systems, as well as exploring new measures and new systems (e.g. the power-law system). In this section, we will summarise our results and consider some directions for future work.

8.1 Logarithmic negativity for the Randbow system

In section 6 we showed that the scaling of the logarithmic negativity of the randbow chain was almost identical to the scaling of the entanglement entropy. In the non-interacting, XX case, we observe a square root scaling that corresponds to the XX case for the entanglement entropy. For the interacting XXX case, we see that the entanglement entropy quickly saturates, which reflects the stability of the bubble regions in this regime. We similarly note that for fixed subsystem sizes but increase intervals r, the negativity of the interacting model scales far more quickly than the non-interacting model, which is is corollary of the previous result.

8.2 Entanglement scaling for the power-law system

For a system with couplings distributed according to a power-law, the scaling of the entanglement entropy and the logarithmic negativity changes significantly. The entanglement entropy at first scales quickly with l, as the short rainbow phase dominates and effects a volume law. However, this rainbow phase is very unstable due to the relatively slow decaying of the couplings, and from that point onwards a logarithmic scaling is observed, in line with the simple disordered model. This was corroborated with the scaling of the exact case for a smaller system size.

For the logarithmic negativity, we observed that the power-law system scales as expected in a very similar way to the simple disordered system. This still displays an area law violation.

8.3 Limitations and Future Work

We have confirmed that area law violations can be achieved even in systems with less spatial inhomogeneity that than exponentially decaying randbow model. This contributes another step in our understanding of one dimensional quantum complex system. However, we were not able to establish any strong analytical results for the power-law system. This is not necessarily intractable given more time, but the power-law expression is not as analytically useful as the exponential expression, so any solution will probably not take the same form as the details of [2]. One could also argue that a better, more rigorous argument for the square root scaling of the randbow entanglement entropy is needed, but the data match very well to the heuristic used here and in [2] that we do need see this as being as important as any sort of quantitative theory of power-law systems in general.

A more exhaustive treatment could have been made of the different ways of measuring the entanglement entropy and logarithmic negativity of the power-law system - for example, calculating the exact solution for the entanglement entropy calculations for a different value of α/δ. However, we have managed to present the main results and we plan on publishing the tools used for these simulations so that they can be verified later if necessary. Furthermore, we have not considered values of Δ outside of 0 and 1, which could also be the subject of future work. Given that the interactions take us back into an area law, which we know is the result of strictly local Hamiltonians, it suggests that the interacting systems could be mapped into a strictly local system for large l and that that could give some further insight.

A Quantum Mechanics and the Jordan-Wigner Transformation

Quantum mechanics is built on state vectors that have a different notion of state to classical state vectors. In a classical system, a state $s(t)$ at time t provides all of the information needed to predict the outcome of an experiment if the experiment were conducted at time t. The mapping of moments in time to possible experimental outcomes is one to one. To have information about the state of a system means that you know what result you will get if you observe the system.

However, in quantum mechanics, the mapping of states to possible experimental outcomes is one to many. A quantum state does not, in general, tell us what we will observe at t - rather, it encodes a range of possible observations that could be made when the experiment happens. The result of the experiment will not be known until the experiment has taken place.

In this section we will briefly summarise the quantum mechanical formalism used throughout the paper, and in particular some details of the Jordan-Wigner transformation as used in 5.5 and 7.2. We will assume the reader is familiar with bra-ket notation and understands the general idea of an operator as it is used in quantum mechanics. For an excellent introduction, see [41].

A.1 Commutators

Most operators do not commute, and the same is true within quantum mechanics. We define the *commutator*:

$$[A, B] = AB - BA \tag{A.1}$$

The *anti-commutator* is defined as:

$$\{A, B\} = AB + BA \tag{A.2}$$

Commutation relations are important in defining the relationships between operators. For example, given the position operators $\hat{x}$ and the momentum operator $\hat{p}$:

$$[\hat{x}, \hat{p}] = i\hbar\mathbb{I} \tag{A.3}$$

This relation between two operators that are Fourier transforms of one another is often referred to as the canonical commutation relation.

A.2 Spin

Spin is a form of angular momentum inherent to quantum particles characterised by a *spin quantum number* s. Restrictions on this spin quantum number imply important properties about different quantum particles. Spin is quantised and takes the form:

$$S = \hbar\sqrt{s(s+1)} \tag{A.4}$$

Where s can be any half-integer. Particles with half-integer spin are *fermions* and particles with integer spins are called *bosons*.

An important property of fermions is that they obey the Pauli Exclusion Principle [42]. Consider a creation operator $a_i^\dagger$ that acts on a vacuum state $|0\rangle$ to create a particle at position i[3]. Adding a particle at position i and another at position j must give us the same state, up to a prefactor:

$$a_i^\dagger a_j^\dagger = \lambda a_j^\dagger a_i^\dagger \tag{A.5}$$

Restricting ourselves without loss of generality to the cases ± 1, we consider the bosonic case of $+1$ first, which implies that the state vector is symmetric under particle exchange. This also implies that:

[3]This explanation of the exclusion principle is due to Blundell and Lancaster [43].

$$a_i^\dagger a_j^\dagger - a_j^\dagger a_i^\dagger = [a_i^\dagger, a_j^\dagger] = 0 \tag{A.6}$$

However, for the *fermionic* case, we have the prefactor -1 and instead the anti-commutator $\{c_i^\dagger, c_j^\dagger\} = 0$, where $c_i^\dagger$ is the fermionic creation operator at i. Mostly importantly, if we set $i = j$ then:

$$c_i^\dagger c_i^\dagger + c_i^\dagger c_i^\dagger = 0 \tag{A.7}$$

$$c_i^\dagger c_i^\dagger = 0 \tag{A.8}$$

Which is exactly the Pauli Exclusion Principle: if we try to create to fermions at the same position, they annihilate and we get nothing at all. This will be relevant when we discuss the Jordan-Wigner transformation in the following section.

A.3 The Jordan-Wigner Transformation

The Jordan-Wigner (JW) transformation maps a system of spins into a system of (free) fermions. This is useful as it opens up a wider variety of technqiues for dealing with disordered, many body problems. We recommend [44] for a thorough overview, and our summary of the JW transformation relies heavily on their layout.

Recall from A.2 that a fermion obeys the Pauli exclusion principle and that one can define a creation operator $c_i^\dagger$ with anti-commutator $\{c_i^\dagger, c_j^\dagger\} = 0$,. Using this, the JW transformation maps spins to fermions according to the following transformations:

$$\hat{\sigma}_j^x = \hat{K}_j \left(\hat{c}_j^\dagger + \hat{c}_j\right) \tag{A.9}$$

$$\hat{\sigma}_j^y = \hat{K}_j i \left(\hat{c}_j^\dagger - \hat{c}_j\right) \tag{A.10}$$

$$\hat{\sigma}_j^z = 1 - 2\hat{n}_j \tag{A.11}$$

where $\hat{n}_j = \hat{c}_j^\dagger \hat{c}_j$ is the fermionic number operator and $\hat{K}_j = \prod_{j'=1}^{j-1} (1 - 2\hat{n}_{j'})$ is a parity adjusting operator. The physical picture here is that we have gone from spins that can be 'up or down' to fermions that can be present or not.

These mappings can be reversed, following [1]:

$$c_i = \left(\prod_{m=1}^{i-1} \sigma_m^z\right) \frac{\sigma_i^x - i\sigma_i^y}{2} \tag{A.12}$$

In the following section we show how this technique can be used to solve the random inhomogeneous chain.

A.4 Using the JW transformation in the exact solution

Again following [1], we define a slightly more general Hamiltonian than equation 3.1 as follows:

$$H_{XX} = \sum_i J_i \left(S_i^x S_{i+1}^x + S_i^y S_{i+1}^y\right) + h \sum_i S_i^z \tag{A.13}$$

Note that this applies strictly to the XX chain, and the additional h term. Using equation A.12 this is immediately transformed into a fermionic form:

$$\mathcal{H}_{XX} = \frac{1}{2} \sum_{i=1}^{L-1} J_i \left(c_i^\dagger c_{i+1} + c_{i+1}^\dagger c_i\right) + \frac{h}{2} \sum_{i=1}^{L-1} c_i^\dagger c_i \tag{A.14}$$

where we have defined the additional anti-commutator relation $\left\{c_m, c_n^\dagger\right\} = \delta_{m,n}$.

One can now assume that each new fermion has individual eigenstates of the form:

$$\eta_q^\dagger|0\rangle = \sum_i \Phi_q(i) c_i^\dagger|0\rangle \tag{A.15}$$

where q labels the different eigenstates and Φ is a vector of amplitudes to be found. The Schrödinger equation becomes:

$$J_i\Phi_q(i+1) + J_{i-1}\Phi_q(i-1) = 2\epsilon_q\Phi_q(i) \tag{A.16}$$

where ϵ_q are single particle eigenvalues per eigenstates q. This is a new eigenvalue problem for a banded $2L \times 2L$ matrix with the couplings J_i on the off diagonals.

The groundstate of the original Hamiltonian will have $L \div 2$ fermions, giving us the following:

$$|GS\rangle = \eta_{q_M}^\dagger \eta_{q_{M-1}}^\dagger \cdots \eta_{q_1}^\dagger|0\rangle \tag{A.17}$$

Multiplying equation A.15 by the relevant operators, we can derive the anti-commutators:

$$\left\{\eta_q^\dagger, c_j^\dagger\right\} = \{\eta_q, c_j\} = 0 \tag{A.18}$$

and

$$\left\{\eta_q^\dagger, c_j\right\} = \Phi_q(j)\delta_{k,j}, \quad \left\{\eta_q, c_j^\dagger\right\} = \Phi^*(j)\delta_{k,j} \tag{A.19}$$

Combining the previous two equations, we can derive the two point function's expected value for the groundstate of the original Hamiltonian:

$$\left\langle c_i^\dagger c_j \right\rangle = \sum_q \Phi_q^*(i)\Phi_q(j) \tag{A.20}$$

This defines a matrix $C_{i,j}$ that can be restricted to some subsystem A for the purposes of analysing a given disorder realisation. In particular, from [45], we can calculate the entanglement entropy:

$$S_A = -\sum_l \left(\lambda_k \ln\lambda_k + (1-\lambda_k)\ln(1-\lambda_k)\right) \tag{A.21}$$

This completes our overview of the technique used in 5.5 to calculate the entanglement entropy exactly.

References

[1] Paola Ruggiero, Vincenzo Alba, and Pasquale Calabrese. "The Entanglement Negativity in Random Spin Chains". May 2, 2016. DOI: 10.1103/PhysRevB.94.035152. arXiv: 1605.00674. URL: http://arxiv.org/abs/1605.00674.

[2] Vincenzo Alba et al. "Unusual Area-Law Violation in Random Inhomogeneous Systems". In: *Journal of Statistical Mechanics: Theory and Experiment* 2019.2 (Feb. 26, 2019), p. 023105. ISSN: 1742-5468. DOI: 10.1088/1742-5468/ab02df. URL: https://iopscience.iop.org/article/10.1088/1742-5468/ab02df.

[3] J. Eisert, M. Cramer, and M. B. Plenio. "Area Laws for the Entanglement Entropy". In: *Reviews of Modern Physics* 82.1 (Feb. 4, 2010), pp. 277–306. ISSN: 0034-6861. DOI: 10.1103/RevModPhys.82.277. arXiv: 0808.3773. URL: https://link.aps.org/doi/10.1103/RevModPhys.82.277.

[4] Don N. Page. "Information in Black Hole Radiation". In: *Physical Review Letters* 71.23 (Dec. 6, 1993), p. 3743. ISSN: 00319007. DOI: 10.1103/PhysRevLett.71.3743. arXiv: hep-th/9306083. URL: https://journals.aps.org/prl/abstract/10.1103/PhysRevLett.71.3743 (visited on 08/24/2022).

[5] Jean Zinn-Justin. "Mean Field Theory For Ferromagnetic Systems". In: *Quantum Field Theory and Critical Phenomena*. Oxford University Press, June 6, 2002, pp. 592–615. DOI: 10.1093/acprof:oso/9780198509233.003.0024. URL: https://academic.oup.com/book/11638/chapter/160554734 (visited on 08/19/2022).

[6] M. B. Hastings. "An Area Law for One Dimensional Quantum Systems". May 14, 2007. DOI: 10.1088/1742-5468/2007/08/P08024. arXiv: 0705.2024. URL: http://arxiv.org/abs/0705.2024 (visited on 08/18/2022).

[7] G. Refael and J. E. Moore. "Entanglement Entropy of Random Quantum Critical Points in One Dimension". In: *Physical Review Letters* 93 (26 I June 29, 2004). DOI: 10.1103/PhysRevLett.93.260602. arXiv: cond-mat/0406737. URL: http://arxiv.org/abs/cond-mat/0406737.

[8] G Vitagliano, A Riera, and J I Latorre. "Volume-Law Scaling for the Entanglement Entropy in Spin-1/2 Chains". In: *New Journal of Physics* 12.11 (Nov. 26, 2010), p. 113049. ISSN: 1367-2630. DOI: 10.1088/1367-2630/12/11/113049. URL: https://iopscience.iop.org/article/10.1088/1367-2630/12/11/113049.

[9] Daniel S. Fisher. "Random Antiferromagnetic Quantum Spin Chains". In: *Physical Review B* 50.6 (Aug. 1, 1994), pp. 3799–3821. ISSN: 0163-1829. DOI: 10.1103/PhysRevB.50.3799. URL: https://link.aps.org/doi/10.1103/PhysRevB.50.3799.

[10] Paola Ruggiero and Pasquale Calabrese. *Entanglement and Correlations in One-Dimensional Quantum Many-Body Systems*. Trieste: SCUOLA INTERNAZIONALE SUPERIORE DI STUDI AVANZATI, 2019.

[11] Asher Peres. "Separability Criterion for Density Matrices". In: *Physical Review Letters* 77.8 (Aug. 19, 1996), pp. 1413–1415. ISSN: 0031-9007. DOI: 10.1103/PhysRevLett.77.1413. arXiv: quant-ph/9604005. URL: https://link.aps.org/doi/10.1103/PhysRevLett.77.1413 (visited on 08/21/2022).

[12] V. Vedral et al. "Quantifying Entanglement". In: *Physical Review Letters* 78.12 (Mar. 24, 1997), p. 2275. ISSN: 10797114. DOI: 10.1103/PhysRevLett.78.2275. arXiv: quant-ph/9702027. URL: https://journals.aps.org/prl/abstract/10.1103/PhysRevLett.78.2275 (visited on 08/21/2022).

[13] Luigi Amico et al. "Entanglement in Many-Body Systems". In: *Reviews of Modern Physics* 80.2 (May 6, 2008), pp. 517–576. ISSN: 0034-6861. DOI: 10.1103/RevModPhys.80.517. URL: https://link.aps.org/doi/10.1103/RevModPhys.80.517.

[14] John F. Clauser et al. “Proposed Experiment to Test Local Hidden-Variable Theories”. In: *Physical Review Letters* 23.15 (Oct. 13, 1969), p. 880. ISSN: 00319007. DOI: 10.1103/PhysRevLett.23.880. URL: https://journals.aps.org/prl/abstract/10.1103/PhysRevLett.23.880 (visited on 08/21/2022).

[15] M. B. Plenio. “Logarithmic Negativity: A Full Entanglement Monotone That Is Not Convex”. In: *Physical Review Letters* 95.9 (Aug. 26, 2005), p. 090503. ISSN: 0031-9007. DOI: 10.1103/PhysRevLett.95.090503. URL: https://link.aps.org/doi/10.1103/PhysRevLett.95.090503 (visited on 08/21/2022).

[16] Charles H. Bennett et al. “Mixed-State Entanglement and Quantum Error Correction”. In: *Physical Review A* 54.5 (Nov. 1, 1996), pp. 3824–3851. ISSN: 1050-2947. DOI: 10.1103/PhysRevA.54.3824. URL: https://link.aps.org/doi/10.1103/PhysRevA.54.3824.

[17] N. Gisin. “Hidden Quantum Nonlocality Revealed by Local Filters”. In: *Physics Letters A* 210.3 (Jan. 1996), pp. 151–156. ISSN: 03759601. DOI: 10.1016/S0375-9601(96)80001-6. URL: https://linkinghub.elsevier.com/retrieve/pii/S0375960196800016.

[18] Alfréd Rényi. “On Measures of Entropy and Information”. In: *Berkeley Symposium on Mathematical Statistics and Probability* 4 (1961), pp. 547–561.

[19] Elliott H. Lieb and Mary Beth Ruskai. “Proof of the Strong Subadditivity of Quantum-mechanical Entropy”. In: *Journal of Mathematical Physics* 14.12 (Nov. 3, 2003), p. 1938. ISSN: 0022-2488. DOI: 10.1063/1.1666274. URL: https://aip.scitation.org/doi/abs/10.1063/1.1666274 (visited on 08/22/2022).

[20] G. Vidal and R. F. Werner. “Computable Measure of Entanglement”. In: *Physical Review A* 65.3 (Feb. 22, 2002), p. 032314. ISSN: 1050-2947. DOI: 10.1103/PhysRevA.65.032314. URL: https://link.aps.org/doi/10.1103/PhysRevA.65.032314.

[21] Luca Bombelli et al. “Quantum Source of Entropy for Black Holes”. In: *Physical Review D* 34.2 (July 15, 1986), pp. 373–383. ISSN: 0556-2821. DOI: 10.1103/PhysRevD.34.373. URL: https://link.aps.org/doi/10.1103/PhysRevD.34.373.

[22] Mark Srednicki. “Entropy and Area”. In: *Physical Review Letters* 71.5 (Aug. 2, 1993), pp. 666–669. ISSN: 0031-9007. DOI: 10.1103/PhysRevLett.71.666. arXiv: hep-th/9303048v2. URL: https://link.aps.org/doi/10.1103/PhysRevLett.71.666 (visited on 08/20/2022).

[23] Don N. Page. “Average Entropy of a Subsystem”. In: *Physical Review Letters* 71.9 (Aug. 30, 1993), pp. 1291–1294. ISSN: 0031-9007. DOI: 10.1103/PhysRevLett.71.1291. arXiv: gr-qc/9305007v2. URL: https://link.aps.org/doi/10.1103/PhysRevLett.71.1291 (visited on 08/20/2022).

[24] Michael M. Wolf. “Violation of the Entropic Area Law for Fermions”. In: *Physical Review Letters* 96.1 (Jan. 13, 2006), p. 010404. ISSN: 10797114. DOI: 10.1103/PHYSREVLETT.96.010404/FIGURES/1/MEDIUM. arXiv: quant-ph/0503219. URL: https://journals.aps.org/prl/abstract/10.1103/PhysRevLett.96.010404 (visited on 08/24/2022).

[25] Pasquale Calabrese and John Cardy. “Entanglement Entropy and Quantum Field Theory”. In: *Journal of Statistical Mechanics: Theory and Experiment* 2004.06 (June 12, 2004), P06002. ISSN: 1742-5468. DOI: 10.1088/1742-5468/2004/06/P06002. URL: https://iopscience.iop.org/article/10.1088/1742-5468/2004/06/P06002 (visited on 08/18/2022).

[26] Pasquale Calabrese, John Cardy, and Erik Tonni. “Entanglement Negativity in Quantum Field Theory”. In: *Physical Review Letters* 109.13 (Sept. 28, 2012), p. 130502. ISSN: 0031-9007. DOI: 10.1103/PhysRevLett.109.130502. arXiv: 1206.3092. URL: https://link.aps.org/doi/10.1103/PhysRevLett.109.130502 (visited on 08/20/2022).

[27] Michael E. Fisher. “renormalisation Group Theory: Its Basis and Formulation in Statistical Physics”. In: *Reviews of Modern Physics* 70.2 (Apr. 1, 1998), pp. 653–681. ISSN: 0034-6861. DOI: 10.1103/RevModPhys.70.653. URL: https://link.aps.org/doi/10.1103/RevModPhys.70.653.

[28] Ferenc Igloi and Cecile Monthus. “Strong Disorder RG Approach of Random Systems”. Feb. 18, 2005. DOI: 10.1016/j.physrep.2005.02.006. arXiv: cond-mat/0502448. URL: http://arxiv.org/abs/cond-mat/0502448.

[29] Ferenc Iglói and Cécile Monthus. “Strong Disorder RG Approach – a Short Review of Recent Developments”. In: *European Physical Journal B* 91.11 (2018). ISSN: 14346036. DOI: 10.1140/epjb/e2018-90434-8. arXiv: 1806.07684.

[30] Barry M. McCoy and Tai Tsun Wu. “Theory of a Two-Dimensional Ising Model with Random Impurities. I. Thermodynamics”. In: *Physical Review* 176.2 (Dec. 10, 1968), pp. 631–643. ISSN: 0031-899X. DOI: 10.1103/PhysRev.176.631. URL: https://link.aps.org/doi/10.1103/PhysRev.176.631.

[31] Shang-keng Ma, Chandan Dasgupta, and Chin-kun Hu. “Random Antiferromagnetic Chain”. In: *Physical Review Letters* 43.19 (Nov. 5, 1979), pp. 1434–1437. ISSN: 0031-9007. DOI: 10.1103/PhysRevLett.43.1434. URL: https://link.aps.org/doi/10.1103/PhysRevLett.43.1434.

[32] Chandan Dasgupta and Shang-keng Ma. “Low-Temperature Properties of the Random Heisenberg Antiferromagnetic Chain”. In: *Physical Review B* 22.3 (Aug. 1, 1980), pp. 1305–1319. ISSN: 0163-1829. DOI: 10.1103/PhysRevB.22.1305. URL: https://link.aps.org/doi/10.1103/PhysRevB.22.1305.

[33] Jean-Philippe Bouchaud and Antoine Georges. “Anomalous Diffusion in Disordered Media: Statistical Mechanisms, Models and Physical Applications”. In: *Physics Reports* 195.4-5 (Nov. 1990), pp. 127–293. ISSN: 03701573. DOI: 10.1016/0370-1573(90)90099-N. URL: https://linkinghub.elsevier.com/retrieve/pii/037015739090099N.

[34] Olexei Motrunich et al. “Infinite-Randomness Quantum Ising Critical Fixed Points”. In: *Physical Review B - Condensed Matter and Materials Physics* 61.2 (June 21, 1999), pp. 1160–1172. DOI: 10.1103/PhysRevB.61.1160. arXiv: cond-mat/9906322v1. URL: http://arxiv.org/abs/cond-mat/9906322 (visited on 08/22/2022).

[35] C. Monthus. “On the Localization of Random Heteropolymers at the Interface between Two Selective Solvents”. In: *The European Physical Journal B* 13.1 (Jan. 1, 2000), pp. 111–130. ISSN: 1434-6028. DOI: 10.1007/s100510050016. URL: http://link.springer.com/10.1007/s100510050016.

[36] Steven R. White. “Density Matrix Formulation for Quantum renormalisation Groups”. In: *Physical Review Letters* 69.19 (Nov. 9, 1992), p. 2863. ISSN: 00319007. DOI: 10.1103/PhysRevLett.69.2863. URL: https://journals.aps.org/prl/abstract/10.1103/PhysRevLett.69.2863 (visited on 08/20/2022).

[37] U. Schollwöck. “The Density-Matrix renormalisation Group”. In: *Reviews of Modern Physics* 77.1 (Apr. 26, 2005), pp. 259–315. ISSN: 0034-6861. DOI: 10.1103/RevModPhys.77.259. URL: https://link.aps.org/doi/10.1103/RevModPhys.77.259 (visited on 08/20/2022).

[38] Ulrich Schollwoeck. “The Density-Matrix renormalisation Group in the Age of Matrix Product States”. Aug. 20, 2010. DOI: 10.1016/j.aop.2010.09.012. arXiv: 1008.3477. URL: http://arxiv.org/abs/1008.3477 (visited on 08/22/2022).

[39] Paola Ruggiero and Xhek Turkeshi. “Quantum Information Spreading in Random Spin Chains”. June 6, 2022. DOI: 10.48550/arXiv.2206.02934. arXiv: 2206.02934. URL: http://arxiv.org/abs/2206.02934 (visited on 08/21/2022).

[40] Maurizio Fagotti, Pasquale Calabrese, and Joel E. Moore. “Entanglement Spectrum of Random-Singlet Quantum Critical Points”. In: *Physical Review B - Condensed Matter and Materials Physics* 83.4 (Jan. 31, 2011), p. 045110. ISSN: 10980121. DOI: 10.1103/PHYSREVB.83.045110/FIGURES/10/MEDIUM. arXiv: 1009.1614. URL: https://journals.aps.org/prb/abstract/10.1103/PhysRevB.83.045110 (visited on 08/25/2022).

[41] J D Cresser. *Quantum Physics Notes*. 2011.

[42] Wolfgang Pauli. “Exclusion Principle and Quantum Mechanics”. In: (1946).

[43] Tom Lancaster and Stephen J Blundell. *Quantum Field Theory for the Gifted Amateur*. 5. Oxford: Oxford University Press, 2014. ISBN: 978-0-19-969933-9.

[44] Glen Bigan Mbeng, Angelo Russomanno, and Giuseppe E. Santoro. "The Quantum Ising Chain for Beginners". Version 1. In: (2020). DOI: 10.48550/ARXIV.2009.09208. URL: https://arxiv.org/abs/2009.09208 (visited on 08/28/2022).

[45] Ingo Peschel and Viktor Eisler. "Reduced Density Matrices and Entanglement Entropy in Free Lattice Models". In: *Journal of Physics A: Mathematical and Theoretical* 42.50 (Dec. 2009), p. 504003. ISSN: 1751-8121. DOI: 10.1088/1751-8113/42/50/504003. URL: https://doi.org/10.1088/1751-8113/42/50/504003 (visited on 08/30/2022).